POLITECNICO DI TORINO

Department of Mechanical and Aerospace Engineering

Master's Degree in Biomedical Engineering

Development of a wearable device for breathing rate monitoring using stretchable sensors

Supervisor:
Prof. Gabriella Olmo
Co-supervisor:
Eng. Alessandro Gumiero

Candidate:
Giovanni Loizzi

ACADEMIC YEAR 2020-2021

Alla mia famiglia

Abstract

In recent years, Wearable Devices (WDs) have gained growing interest in detection of human vital parameters, from simple activity trackers to more complex systems capable of providing active interaction with the human body. This is also due to the spread of IoT systems, which allow the efficient data processing provided by various devices. Despite the development of even smaller and more powerful rigid electronic devices, the spread of stretchable sensors has attracted attention because of their skin-like characteristics, their multiple application fields and their environmental impact.
A wearable device using flexible and stretchable sensors, based on strain-response mechanism, to monitor breathing rate is designed and analyzed in this research study. The impedance variation has been evaluated connecting two evaluation boards with a stretchable sensor, developed by Uppsala University. The STM32Cube MX software and the µVision®5 IDE, property of ARM, have been use to program the MCU.
The performance of the developed device is evaluated in several body positions: sitting, standing and walking.
The acquired sensing signals are then filtered and breathing parameters are extacted on Matlab R2021a. Afterwards, the related final results are discussed and compared with those extracted from the Pulse Sense device, a wearable device developed by STMicroelectronics.
Statistical analysis are performed and confirm that there is no significant difference between the measurements acquired by the devices.
The stretchable sensor used shows high stretchability, and excellent fit for wearable applications, leading to the possibility of further integration into more complex wearable sensing systems.

List of acronymus

AD Analog Device

ADC Analog-to-digital converter

AFE Analog Front End

bpm breath per minute

bps bits per second

BR Breathing rate

CS Chip Select

ECG Electrocardiogram

EDA Electrodermal activity

EDR ECG-Derived Respiration

EP Elastomeric Plethysmography

ERV Expiratory Reserve Volume

FIFO First in, first out

FIR Finite impulse response

GPIO General-purpose input/output

IDE Integrated Development Environment

IP Impedance Plethysmography

IRV Inspiratory Reserve Volume

IJP Inkjet printing

I2C Inter-Integrated Circuit

MAE Mean Absolute Error

MISO Master in, slave out

MOSI Master out, slave in

PPG Photoplethysmography

RIP Respiratory Inductive Plethysmography

RV Residual Volume

SD Standard Deviation

SDMMC Secure Digital Multimedia Memory Card

SPI Serial peripheral interface

ST STMicroelectronics

T Breathing period

Ti Inspiratory time

Te Expiratory time

TIA Transimpedance amplifier

TLC Total Lung Capacity

UART Universal Asynchronous Receiver-Transmitter

USART Universal Synchronous-Asynchronous Receiver/Transmitter

USB Universal Serial Bus

VC Vital Capacity

WD Wearable Device

WFS Wearable and flexible sensors

Contents

List of Figures

Chapter 1

Introduction

1.1 Telemedicine

The term telemedicine was first coined in the 1970s and refers to the use of ICT to enhance patient health status by facilitating access to medical care and information. Over the years, there have been several definitions of telemedicine, the World Health Organization describes that as:

"The delivery of health care services, where distance is a critical factor, by all health care professionals using information and communication technologies for the exchange of valid information for diagnosis, treatment and prevention of disease and injuries, research and evaluation, and for the continuing education of health care providers, all in the interests of advancing the health of individuals and their communities" [1].

A study conducted in 2007 found that there are more than 104 peer-reviewed definitions of telemedicine, but all of them underline that telemedicine is an open and continuously developing science, because it includes new progress in technology and responds and adapts to constantly evolving health needs and backgrounds of societies. The main elements that characterize telemedicine are listed:

- Its aim is to offer medical support.
- It is designed to overcome geographical barriers, connecting users in different parts of the world.
- Its aim is to improve health outcomes.
- It includes the use of various types of ICT.

Depending on the timing of the information transmitted and the involvement of individuals, telemedicine applications can be distinguished into two different types: *store-and-forward* and *real time* telemedicine.

The former involves the sharing of previously recorded information between two or more people at different time. For example, the caregiver or the patient sends data to a health professional, who then analyzes it, giving an opinion on diagnosis and optimal management. The latter implies that the people involved are both present at the same time for an immediate exchange of information, as in the case of video-conferencing.
In both *store-and-forward* and *real time*, synchronous and asynchronous telemedicine, relevant information may be exchanged in different formats, like text, images, audio, or still video. These two basic telemedicine methods are used for a variety of services in different settings, including teledermatology, telepathology, and teleradiology.
Variability in diagnosis, clinical management, and delivery of care services around the world are just a part of the services where telemedicine has a major influence. Indeed, it can improve the quality, access, and cost of these services. In particular, telemedicine can help developing countries, reach remote or rural areas with few health care services and personnel, and overcome barriers such as time and distance.
In addition, the use of this new system shows that there are also socioeconomic benefits for patients, families, health care professionals and the health care system, including improved patient-provider communication and educational opportunities. Even so, telemedicine has not been fully accepted by the global community yet. There are several reasons for this rejection; some refuse to use services different from traditional approaches or from indigenous practices, while others do not have the ICT literacy to effectively use telemedicine approaches. A lack of studies documenting economic benefits and cost-effectiveness has also contributed to the slow uptake of telemedicine.[2]
Despite the many barriers, telemedicine deployment grew dramatically during the pandemic. However, at the same time also new problems and risks that need to be managed have emerged, specifically with respect to information security and privacy. A raised level of risk of cyberattacks towards the healthcare sector and organizations doing research on COVID-19 have been noted by government agencies. Successful cyberattacks negatively impact hospital operations, delay access to clinical services and lead to significant financial losses.
Protection against these attaks is complex, and requires a multi-disciplinary, multi-stakeholder strategy. Awareness is an important first step in countering these attaks, and can take the form of education, employee training, and simulated cyberattacks toward establishing a culture of security. Ultimately, while health systems should assign significant resources to improve telemedicine capabilities, health care organizations must ensure that these new capabilities are secure and protect the privacy of individuals. [3]

1.2 Wearable devices and their application

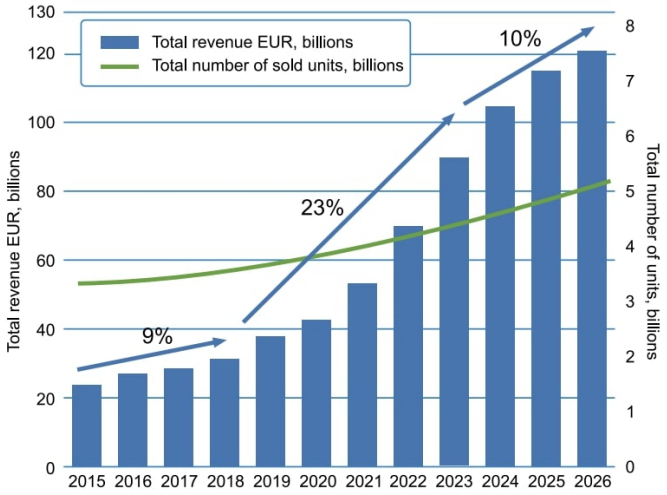

Figure 1.1: Wearable market growth forecast.

Wearable Devices (WDs), and in particular Wearable Health Devices (WHD), have gained enormous attention in recent years. This success is due also to the spread of "Internet of Things" (IoT), which allowed the connection of different objects and industrial apparatus to a data network, collect and process information from them to create new services.
"Wearable" means whatever a subject can wear, as shirt, socks, watches, glasses or patches, without affecting daily life. The concept of wearability finds particular relevance in fields such as monitoring for health, wellness and fitness/sports.

Comparing these to current cell phones and tablets, one can see that the main value carried by WDs is that they can provide monitoring and scanning support, including biofeedback or other sensory physiological features such as biometry-related ones restricted by their battery constraints. In addition, they are more convenient, seamless, portable, and can offer hands-free access to electronics.
The variety of information acquired and elaborated in a wearable environment can provide useful information in order to improve the user's quality of life.
Carrying a WD can potentially predict disease through continuous health monitoring and even inform the doctor automatically in order to take action and actively prevent the incoming threat. Sleep patterns, heart rate, stress level or body temperature are parameters that are already possible to measure even through simple activity trackers and could be used to improve the health status of any individual. The most widely used WDs to date are sports trackers, smartwatches, on-body cameras, but a new generation of wearables is coming, thanks also to stretchable electronics.
The spread of WDs was also driven by the implementation of various crowd-sensing and contact-tracing platforms needed to mitigate the COVID-19 epidemic. The

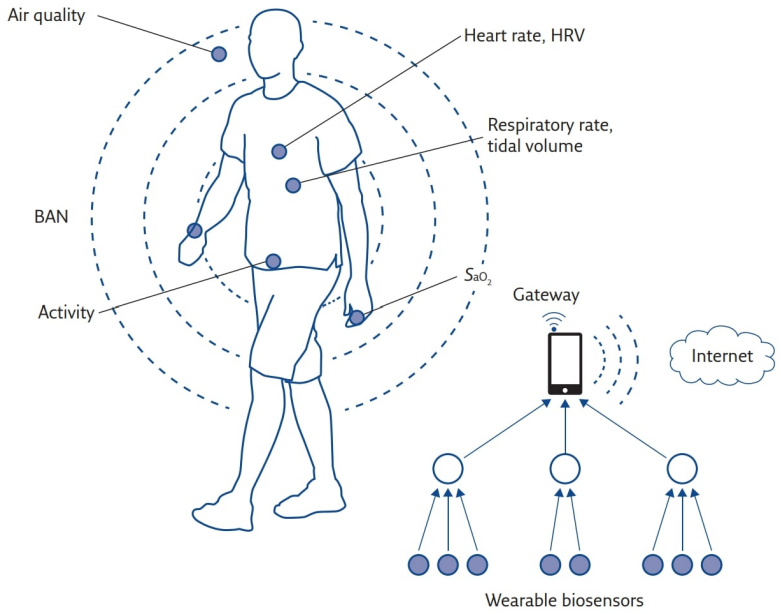

Figure 1.2: Design of a system used to monitor patients through wearable sensors.

spread of wearables is therefore set to increase steadily over the next few decades, with a predominant progression from sports bracelets and trackers to smarter, feature-rich devices.

From an economic viewpoint, the wearable market is expected to continue to grow exponentially in the coming years. The forecast is at more than 20% growth rate annually, and the market is expected to reach over 40 billion EUR per year in the next 5 years with more than 150 billion EUR by 2028 (Figure 1.1) [4].

Different WDs can be also connected to each other, as it happens in Body Area Networks (BANs) or body sensor networks (BSNs). BANs are composed of a network of WDs that could be placed on the subject's skin, implanted inside the body, or embedded inside clothing. In cardiac monitoring, for example, when continuous deployment is required, sensors embedded in implantable defibrillators or pacemakers are used. A typical architecture of a monitoring system involves wearable devices communicating with stationary devices (wireless local area network) or gateway devices (mobile phone) that then allow sensor data to be transmitted to remote locations. Once the measurements have been completed, they can be stored locally on a monitoring WD for later transmission or transmitted directly (e.g., via the public telephone network) to a medical center. Regardless of the patient's location, the information will be accessible via the Internet in every case [5].

The success of wireless BSN systems is based on using low-power measurement and transmission systems and providing a platform to establish a personalized health monitoring system, with the goal of recording an individual's chronic and acute events [6].

In this context, wearable systems may offer informations not only to health professionals and patients. WDs could be used to provide support for post-operative

rehabilitation, recovery, and autonomy for an elderly person. They can be used to monitor and track the condition of patients in cities or developing areas , thus reducing the amount of workload of healthcare staff and the cost of medical services and increasing , the efficiency of the entire healtcare system and patient comfort. Mortality can be reduced with proper instructions given to patients at the right time.
Moreover, trends and improvements in performance of healthy subjects performing recreational and sporting activities could be monitored. Smart fabrics or sensorized clothing could be used to help sports professionals in assessing performance , body kinematics and physiological parameters or to study an athlete's reaction to a given external stimulus.
The advancement of WDs is also due to the development of a larger quantity of wearable sensors, which combined with rigid electronics allows to reach every part of the human body. As mentioned above, a new wearable technology is gaining success: it is intimately associated with clothing and tissues and must be washable, stretchable, printable or transparent.

1.3 Stretchable and soft electronics

Stretchable sensor were introduced in the early twenty-first century and immediately attracted the attention due to their characteristics, which improved the capabilites of traditional rigid electronics. Indeed, lots of soft, stretchable, flexible electronic devices merged with polymeric substrates have shown to be useful for the acquisition of biological signal for healthcare monitoring. Moreover, stretchable sensors easily notify certain health conditions without asking medical workers to connect to smart devices, thereby not only improving diagnostic procedures but also providing health information by monitoring body conditions. In order to perform their task, they are fixed on the skin surface.
Despite progress in the performance and miniaturization traditional electronics, which is usually consisting of rigid materials that have little flexibility and extensibility, are severely limited when interfacing with non-static and non-planar surfaces. Specifically, the different physical properties at the electronic-skin interface are the most challenges to make the next generation skin integrated electronics.[7]
Skin is considered one of the main organs of the body [8] and it can both transmit and provide biological signals. The quality of the bio-adhesion between the soft, stretchable sensor and the skin is an important parameter to consider. Indeed, a good contact means good signal acquisition results. To overcome this issue electrodes with gel, straps or mechanical clamp are used, but these solutions influence the accuracy of health monitoring. But the skin-sensor adhesion is only one of the main characteristics of a good wearable sensor.[9]
Mechanical considerations have to be also considered. The terms "epidermal", "skin-like" and "electronic tattoo" refer to skin-mounted devices with physical properties similar to the epidermis and enabling at the same time robust contact. It is important that the electronic device has elastic modulus similar to that of skin and like it can also deform elastically up to 15%. Therefore, any epidermal electronic device must be able to not only bend to conform to the topography of the skin, but also to stretch to adapt to tensions during natural body movement.
As Figure 1.3 shows, polymeric materials have an elastic moduli similar to the skin, instead of material that are used usually in electronic devices (silicon, gold, etc.). So, thanks to recent advances in nanotechnology, structural optimization of the device through the integration of materials such as polymers, metals, and semiconductors was possible.
Anyway, also electronic properties have an important role. As said before, organic materials seem to be the best choice to interface with the skin because of their biocompatibility and also thanks to their low production's cost, but they do not have good electrical mobility and they are chemically unstable. Gold and platinum are the most widely used metals due to their low contact impedance and chemical inertness.

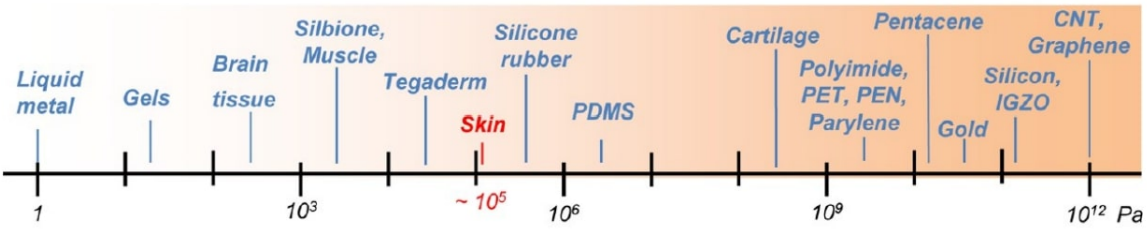

Figure 1.3: Comparison of different elastic moduli for different materials including human skin

Because of its low electrical resistivity, copper is widely used to interconnect several modules.
However, liquid metal alloys embedded in soft elastomers are now also a realistic possibility for stretchable interconnects [7]. The terms "liquid metal" and "liquid alloy" refer to a metal or alloy which is in a liquid state at room temperature. Liquid metals and liquid alloys, characterized by simultaneously holding thermal and electrical properties comparable to those of rigid metals, as well as mechanical and dynamic properties of liquids, naturally offer advantages that are particularly well suited for applications in the field of soft electronics. The ability of low viscosity liquid alloys to undergo stress-free deformation allows for soft electronics with interconnects that have relatively large cross-sections, which can significantly reduce the resistance of the circuits compared to stretchable or flexible electronics made with rigid metal interconnects. A liquid is able conform to surfaces that are arbitrarily curved in space and continuously changing in time, making liquid alloys a good candidate for use in epidermal electronics and as tissue contacting electrodes with a low contact resistance [10]. Mercury is a commonly known liquid metal, but it is toxic and therefore not widely used as a wearable stretchable material. Therefore, much attention has been paid to low toxicity Gallium-based liquid metals such as gallium indium eutectic (EGaIn) and Galinstan (GaInSn).[11]
Based on the methods of attaching WDs to the skin and their functionality, three types of flexible device integration strategies can be categorized:

- Temporary epidermal tattoos, which use silicone materials, like PDMS, Ecoflex, etc., as substrates. These have similar mechanical properties, such as elastic modulus, to that of skin. Also other polimeric materials could be used as substrates or protective layers. However, many digital function are limited by the complexity the complexity of fabricating high-performance integrated circuits

- Hard-soft integration, which combines commercially chips with soft, flexible patches for integration with the skin.

- Functional substrates, where thin-film electronics are combined with different functional substrates for application-specific sensors

Finally, in [12] a comparison from an environmental point of view between stretchable electronic devices and rigid electronics-based devices is conducted. Specifically, the objective of this study is to understand which device and associated manufacturing process is most sustainable. The main contributor to environmental impacts is provided by the raw materials of which the devices are composed. The flexible electronic has the lowest impact due to the limited raw materials that are consumed in the PCB manufacturing process. On the manufacturing processes side, the overall amount of electricity used as a result of the manufacturing steps is considered and the higher environmental impact of rigid electronics is demostrated.

Anyway, what are the healthcare application areas for these?
In accord to the requirements of various individual, stretchable sensor are used in different healthcare application, like body temperature detection, heart rate and muscle monitoring. In this thesis work a stretchable strain sensor is used to monitor breath rate.

1.4 Respiratory System

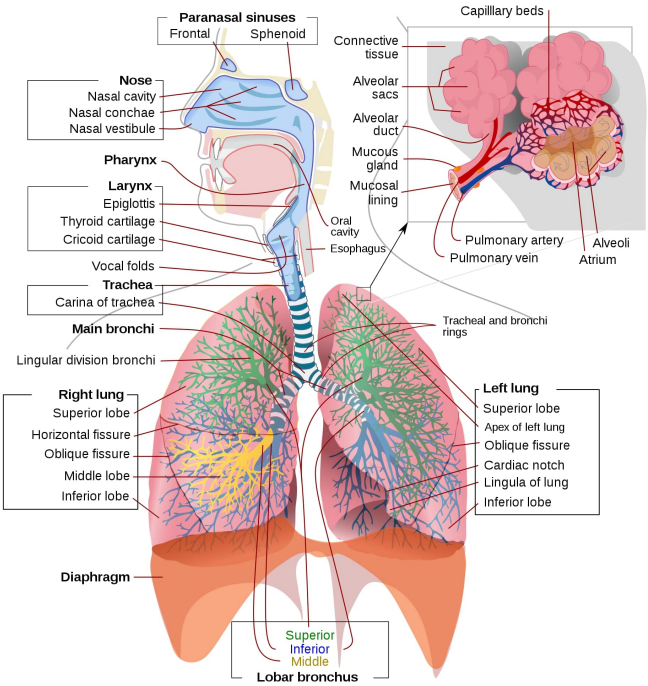

Figure 1.4: A schematic view of the human respiratory system with their parts and functions.[13]

Breathing rate (BR) is a vital parameter that is related to, therefore regulated by, multiple physiological and neural activities. BR plays an important role in the detection of various cardiovascular and respiratory diseases, as well as relevant clinical events.

1.4.1 Basic of Respiratory System

The respiratory system is a biological system comprising different structures and organs that aim to three vital functions: activate the ventilation pump, transport gases in the airways and ensure the gas exchange.
Its basic structures could be divided in accord to their functions into two different groups: the airways, which transport gases from the openings to the lungs, and the lungs, in which the gas exchange takes place.[14]

The airways are composed by the airways openings (nose and mouth), paranasal sinuses, pharynx, larynx, trachea and bronchi; then the bronchial tree continues branching in the lungs until reaching the level of terminal bronchioles that bring to alveolar sacs, in which clusters of alveoli form the spongy structure of the lungs. The air (or the gases) flows into these structures to achieve lungs and alveoli during the inspiration, and in the opposite direction during the expiration.
Alveoli are wrapped in blood vessels allowing gas exchange due to concentration

gradients and diffusion phenomena. At this stage carbon dioxide is released by the bloodstream to the atmosphere and the oxygen in absorbed by the bloodstream.
It is now evident that is necessary a force to create the gas flow in the airways. This force, applied as a difference of pressure, is provided by other structures: the respiratory muscles of the ribcage and the diaphragm, which is the main respiratory muscle and is situated in the abdomen.
The coupling between lungs, diaphragm and rib cage is ensured by the pleura, which is a membrane composed by two layers separated by a thin pleural cavity: the inner layer covers the lungs, the outer layer is attached on the chest wall. In this way, when respiratory muscles are activated for the inspiration, the chest wall gets bigger and lungs follow the chest wall movements due to the pleural coupling, leading to a negative lung pressure and to a consequent air flow towards the lungs.
When inspiration and the action of respiratory muscles end, the rib cage collapses to reach the equilibrium position and the gases flow in the opposite direction.
The modes of breathing are essentially two: the *quiet breathing* that, related to the contracted muscles, which can be diaphragmatic or costal and the *forced respiration*, where more muscles are involved.
Moreover, can be observed that the inhalation is an active and voluntary action, while the exhalation is active only in the forced, because in the exhalation at rest is observable the physiological restoration of the original dimensions (elastic return).

1.4.2 Measurements of respiratory signal

Observing respiratory parameters is crucial for monitoring of the physiological respiratory system mechanical conditions.
To evaluate them, the most commonly used indexes are changes in absolute volume and gas volume in the lungs that can be calculated during respiratory testing.
The maximum volume of gas that can be accumulated in the lungs by a healthy subject after maximum inhalation is the *Total Lung Capacity* (TLC), which can be up to 6000 ml in males. It is formed by four volumes: *Tidal Volume (Vt)*, *Inspiratory Reserve Volume*(IRV), *Expiratory Reserve Volume* (ERV) and *Residual Volume* (RV):

- Vt refers to the air that moves into and out of the lungs with each quiet breath (approximately 500 ml).
- IRV is the volume of gas that can be forcefully inhaled in addition to the current volume (approximately 2100-3200 ml),
- ERV refers to the air that can be maximally exhaled from the lungs after a tidal expiration (almost 1000-1200 ml).
- RV is the smallest lung volume a subject can reach and refers to the air remaining in the lungs after maximal expiration (approximately 1200 ml).

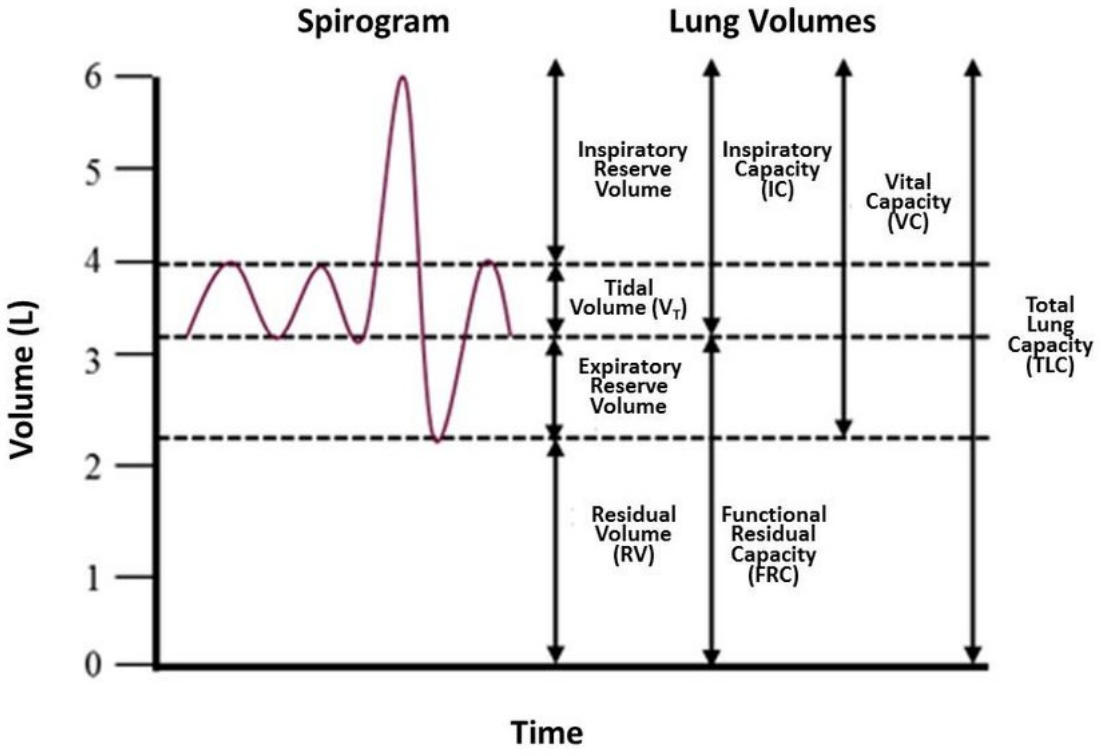

Figure 1.5: Standard lung volumes and capacities from a spirometer trace. [15]

The volume of gas present in the lung at the end of a quiet expiration, when respiratory muscles are relaxed, is the *Functional Residual Capacity* (FRC).
The difference between TLC and RV is the Vital Capacity (VC). In particular, it determines the maximal volume change the lungs can sustain during a voluntary respiratory manoeuvre. VC can be divided in two distinct parts: the expiratory reserve volume (ERV = FRC - RV), previously described, and the Inspiratory Capacity (IC = TLC – FRC or IRV - Vt), the total amount of air that can be inspired after a tidal expiration [16].
Figure 1.5 shows an example of a volume-time spirogram graph with the indexes listed.
In addition to volumes, temporal parameters of respiration should also be considered. The most commonly used are *respiratory rate* or frequency (f or RR), generally defined as breaths per minute (BPM); *Inspiratory time* (Ti), seconds required to reach a maximum volume in one breath; *Expiratory time* (Te), which refers to the seconds to reach the minimum volume after the peak volume; *Breathing period* (T), defined as the time during which the breath is done (seconds elapsed between two sequential minima).
Lung volume changes measurements can be obtained considering two different approches. The first one consist of measuring gas volume changes in the body during breath, using plethysmograph techniques. It will be discuss in the next paragraphs. The second approch, also known as spirometry, requires of measuring the amount

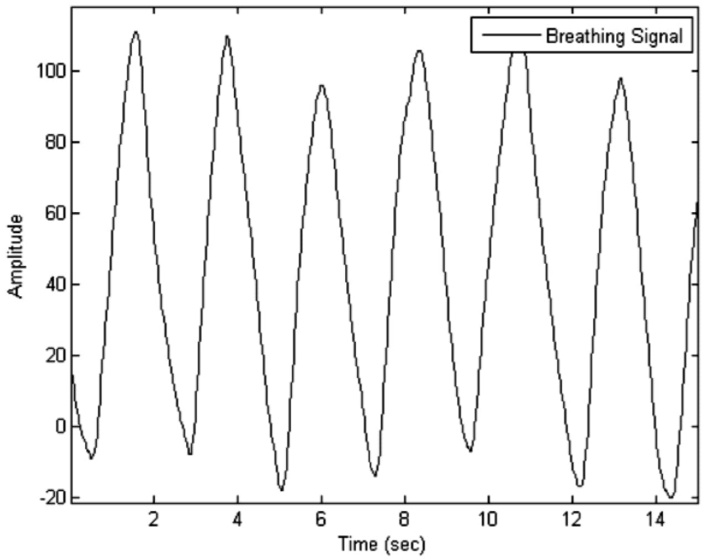

Figure 1.6: Example of respiratory signal of 15 sec of normal breathing with baseline-drift.[17]

of gas through the airways opening and calculating the corresponding volume in the lungs. This represents a physical integration of the flows through the mouth and it is obtained using a spirometer.
A spirometer is an device that is able to obtain directly the volume of air moved or measures airflow by using a flow sensing device, such as a pneumotachometer or a tube containing a fixed resistance to flow. Spirometry is the one of the most generally used lung function screening tests. It is widely used for diagnosing, monitoring and evaluating symptoms or abnormal laboratory tests, the effect of disease on pulmonary function, pre-operative risk and stratification, or simply as a tool in epidemiologic and clinical research. Spirometry needs a voluntary manoeuvre in which a seated patient is asked to inhale maximally, through a mouthpiece and with a nose clip, from tidal respiration to total lung capacity and then rapidly to exhale to the fullest extent until no further volume is exhaled at residual volume. Since spirometry is an expiratory maneuver, it measures exhaled volume or vital capacity but does not measure absolute volumes such as residual volume, functional residual capacity (resting lung volume), or total lung capacity.
Without spirometer, the respiratory signal that can be achieved from an healty subject is morphologically similar to the one shown in the Figure 1.6. The signal morphology shown is similar to that detected by plethysmography techniques. It is comparable to to a sinusoid of period between 3.3 and 5 s having therefore a frequency between frequency between 0.2 and 0.3 Hz. These values identify the absence of pathology, therefore of a subject whose breathing can vary between 12 and 18 acts/min. In this signal the ascending strokes represent inhalations and the descending strokes represent exhalations, while the depth of the breath depends on the subject and the activity that being carried out. In fact, according to the type

of breathing and the state of the individual, this signal can have different amplitude and the peaks can be more or less close together in time.
Therefore, from the respiratory rate and the morphology of its signal it is possible to trace any alterations that can be examined.
In this work a technique close to the plethysmographic one will be analyzed to obtain respiratory parameters.

1.4.3 Respiratory Disordes

Regardless of the type of breathing, the system adapts to provide the appropriate amount of oxygen and to do this it can both can change both the number of breaths in a unit of time and the amount of air that moves with each breath.
Children have a higher respiratory rate than adults. Due to the delicate birth conditions some babies are born with, monitoring of breathing can prevent any accidents due to sleep apnea. The median respiratory rate in the first two years is reduced from 44 bpm at birth to 26 bpm during their second year of life [18].
The typical changes in respiratory rate for an adult at rest are 12 to 20 bpm [19]. However, an elderly individual with more than 28 respirations/min is deemed tachypneic.
Several things can be caused by respiratory disorders.
Usually, a high or low respiratory rate is caused by sports activity and is not a warning that there is something wrong, but these variation can be used to optimize the training or to prevent health problems.
Respiratory rate variations can be used in the study of human emotions: fear, sadness, happiness or surprise could influence it. Breathing monitoring may also contribute to real time recognition of emotions to obtain information in several fields, like to assess the level of safety of the drivers or to monitor the level of attention in a learning process.
Moreover, the effect on the working field is studied: monitoring workers' breathing can be useful in order to consider work-related hazards and consequently plan preventive actions to be taken before any problems appears.[20]
From a medical perspective, although frequently overlooked, an abnormal respiratory rate, especially if it is too fast, may be an indicator of a health problem.
It has been demonstrated that clinical problems, such as cardiac arrest or admission to an intensive care unit, can be predicted by breathing rate, which can distinguish between healthy and unhealthy patients better than pulse and blood pressure measurements. [21].

Some of the important respiratory disordes are described here:

- *Hyperventilation*: it occurs when breathing is faster than necessary and an excessive amount of carbon dioxide is released. The equilibrium in the blood is out of balance. Hyperventilation could be triggered by exercise, anxiety or asthma. It can make the subject feel dizzy, weak or confused.

- *Dyspnea*: it occurs when breath are too short, so the body could not get enough air. Heart and lung problems are often related. The appearance of dyspnea can be a symptom of something serious such as a heart attack or asthma attack. It can also occur if the person is obese, in poor health, or is at high altitudes.

- *Bradypnea*: it occurs when the subject's breathing is slower than normal. It could mean that the body of the subject is not getting enough oxygen. Metabolism disorders or other problems, such as carbon monoxide poisoning or sleep apnea may be symptoms caused by bradypnea.

- *Tachypnea*: that is the opposite of bradypnea. It means that the subject's breathing is at a rate higher than normal. It may be a symptom of a disease that limits the amount of air the lungs are able to take in, such as COPD or pneumonia. More breaths are therefore helpful in keeping the same amount of oxygen flowing through the body.

- *Hyperpnea*: it occurs when the subject breath more air but not necessarily faster. This condition can be triggered by exercise or by medical conditions that limit the body's absorption of oxygen, heart failure or sepsis (a severe overreaction of the immune system) are examples [22].

1.5 State of the art

Figure 1.7: Several commercially available wearable devices and their position to estimate breathing parmeters [23]

Despite the development of BR measurement technologies, BR is still often neglected or inaccurately estimated in clinical practice.
Recently, wearable and flexible sensors (WFS) have been widely applied in medical and healthcare areas.[24]
The respiratory wave extracted from the variation of the volume of the thorax during the phases of inhalation and exhalation allows to extract the BR. The thoracic expansion together with the muscular signs allow to calculate the respiratory effort. The study of these data in sports, especially in professional athletes, can help to improve respiratory performance[25][26].
In recent years, wearable devices developed to assess and monitor the respiratory rate of a patient's respiratory system use different techniques.
There are mainly three plethysmographic methods to obtain the respiratory rate:

- Elastomeric Plethysmography (EP). It is a technique in which an elastic belt is attached around the chest or abdomen. When the chest or abdomen expands or contracts, the belt is deformed and the deformations are measured and converted to a voltage. using a piezoelectric sensor [23].

- Impedance Plethysmography (IP). It refers to a technique that measures the variation in impedance as the cross section of the body expands and contracts. A weak alternating current is passed through electrodes placed on the body in order to measure these changes [23].

- Respiratory Inductive Plethysmography (RIP). This technology's principle is based on a loop wire with current that generates a magnetic field normal to the loop orientation [27].

Other methods are being developed such as:

- Using Accelerometers. The triaxial accelerometer is used as an inclinometer to reflect the movement of the abdomen or chest caused by respiration. This technique is usually used in addition to other techniques in order to refine measurements.
- Using the ECG Signal. This method derives the respiratory rate directly from the ECG signal. ECG-derived respiration (EDR) is the name of the technique that derives respiration rate by measuring the ECG fluctuation. It is based on a specific process known as sinus arrhythmia, which is the modulation of the ECG by the breathing process [28].
- Using Pulse Oximetry: Blood oxygen saturation (SpO2) is also a parameter related to breathing. When you breathe in, oxygen binds to hemoglobin in red blood cells. Arterial blood carries oxygen throughout the body. The percentage of hemoglobin in the blood, which is saturated with oxygen, can be measured through the use of a pulse oximeter. This percentage is called blood saturation, or SpO2. An oximeter simultaneously displays the SpO2 level, as well as the pulse rate and the plethysmogram [28].

1.5.1 Available Respiration Rate monitoring devices

Some of the available Respiration Rate monitoring devices are listed below:

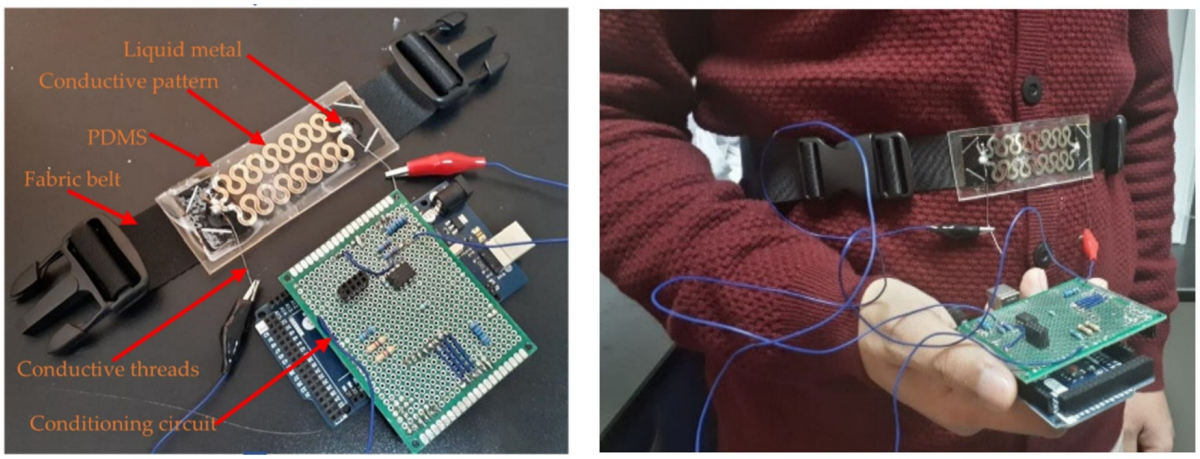

Figure 1.8: The Inkjet printing (IJP) breathing rate (BR) sensor and the related electrical circuit to acquire signal.

Al-Halhouli Inject-Printed Strain Sensor This device is a low cost and easy to use wearable BR sensor. Inject printing (IJP) is a promising technology for the development of wearable and stretchable sensors. This particular device has a substrate made of polydimethylsiloxane (PDMS), that is widely used to create stretchable circuits. A conductive silver nanoparticles ink is injected into the PDMS substrate through an Inject printer. The pattern chosen to support up to 25% in accord to [29] is the horseshoe pattern, illustrated in the Figure 1.8.

During breathing, the variation of resistance of the sensor is considered, which increases during inspiration and decreases during exhalation, due to the change of volume in the rib cage or abdomen. Resistance changes are measured through a Wheatstone bridge-based circuit with three fixed resistors and an instrumental amplifier. The data is then collected by an Arduino microcontroller to obtain the BR. The results are then compared with those extracted from a reference device, the so-called e-Health nasal sensor, an airflow sensor that senses the thermal changes in the nasal airflow. The measurements confirm that this sensor can be used for BR monitoring, indeed a negligible error compared to the reference sensor has been detected. The IJPT sensor is promising in achieving reliable BR monitoring for COPD patients where the use of this sensor would contribute to mitigate the frequency and severity of COPD exacerbation symptoms by early detection of abnormal physiological measurements including the respiratory rate [30][31][32].

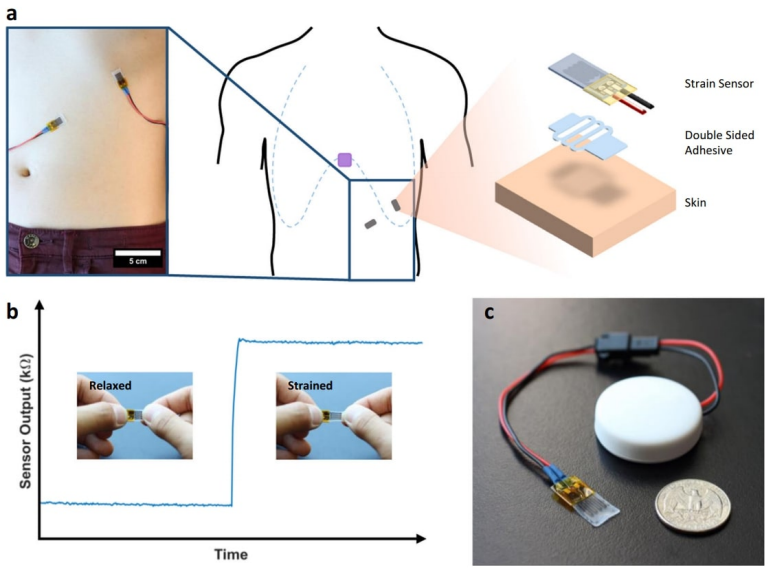

Figure 1.9: **a.** Strain sensors fixed on the body. The accelerometer positioning is also shown (purple square). The exploded figure on the right shows the placement of the sensor on the skin. **b.** Resistance variations of the sensor obtained through the wireless Bluetooth module. **c.** The Bluetooth module with the strain sensor used [33].

Khine Lab's Wearable Respiratory Sensor This device is able to monitor both respiration rate and volume rate through strain sensors located on the ribcage and abdomen. The detection method consists of the guided fracture of the metal thin film to increase the variation of the deformation resistance. The sensors have small dimensions measuring 21 mm by 10 mm by 0.5 mm and were placed perpendicular to each other to minimize crosstalk. A double-sided film, approved by FDA ,is used to attach the sensors to the skin. However, the tape is not inherently stretchable, so some cuts are made on the film to allow it to stretch with the skin. Any movement during all tests were detected by a 3-axis accelerometer placed under the sternum. During the test, a spirometer, as the gold standard device, was used to measure the respiratory volume. Data is trasmitted by embedded sensors via Bluetooth to a smartphone app.
Using this device, high-risk patients, such as COPD or asthmatic patients, can be monitored continuously, acute changes in respiratory parameters can be reported so that the problem can be quickly managed [33].

Figure 1.10: RespiraSense™ device and usage example. A non-invasive pulse oximeter can also be used to monitor oxygenation.

RespiraSense™ RespiraSense™, by PMD Solutions, is a wearable, wireless, motion-tolerant device designed to monitor respiratory rate of acute patients. It alerts medical staff with an alarm for abnormal breathing, as the changing pattern of this is one of the first signs of possible deterioration of the patient from conditions such as respiratory impairement, worsening of pneumonia, increased severity of sepsis, and incoming heart attacks. RespiraSense™ predicts hypoxia and pyrexia 12hrs in advance in COVID patients.

The sensing technology used by the device consists of an array of assembled piezoelectric films. Deformations of the thoracic and abdominal surfaces caused by breathing movements are detected by the sensor and converted into an electrical signal. By monitoring the rate of these changes, the respiratory rate can be traced. The data collected are trasmitted to the mobile application through Bluetooth. Study showed that for measurements obtained at rest a mean BR of 19.3 (SD 4.89) for manual measurements compared to mean BR of 20.2 (SD 4.54) for measurements obtained with capnography and mean BR of 19.8 (SD 4.52) with RespiraSense™. The resting results of the RespiraSense™ device compared with those derived from capnography showed a bias of 0.38 and limits of agreement from 1.0 to 1.8 bpm. [34].

Chapter 2

Prototype Development

In this work a new health monitoring device is developed to monitor breathing rate of a patient. Stretchable sensors, developed by Uppsala university, are used to this aim. The impedance variation of them is evaluated and measured by a multimodal sensor front-end ADPD-4000Z by Analog Device and acquired thanks to the STWIN SensorTile wireless industrial node (STEVAL-STWINKT1), which is an evaluation board that simplifies prototyping and testing of advanced industrial IoT applications.
Once data is acquired with these devices, it is processed and vital parameters are extracted. The entire system developed is shown in the figure Figure 2.1.

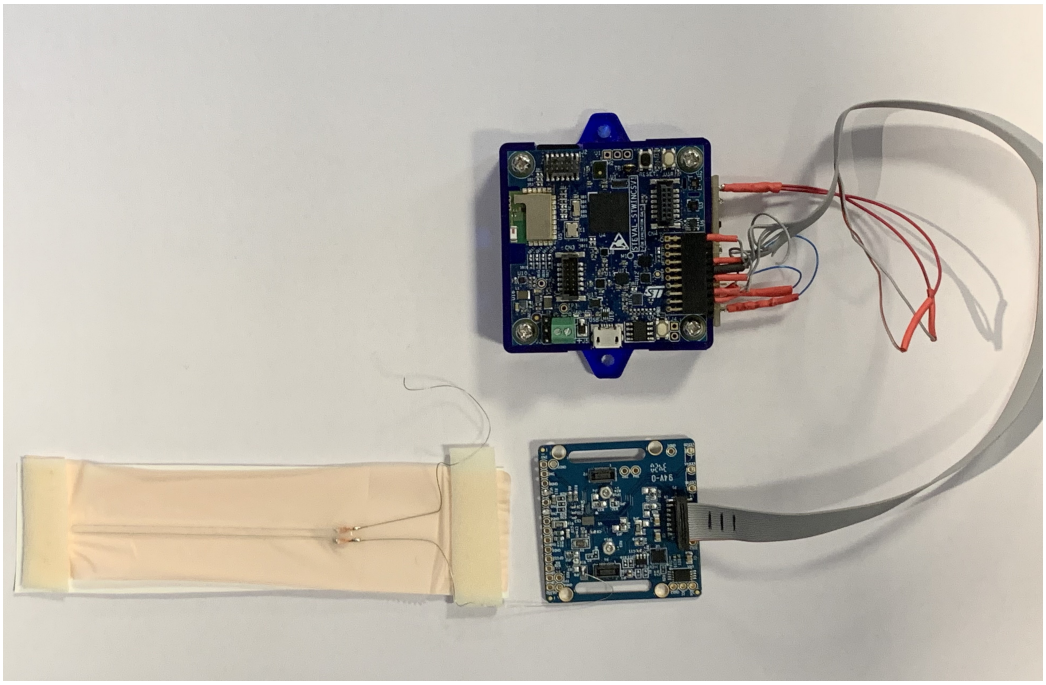

Figure 2.1: Complete setup for breathing rate monitoring

2.1 Hardware Design

2.1.1 STEVAL-STWINKT1

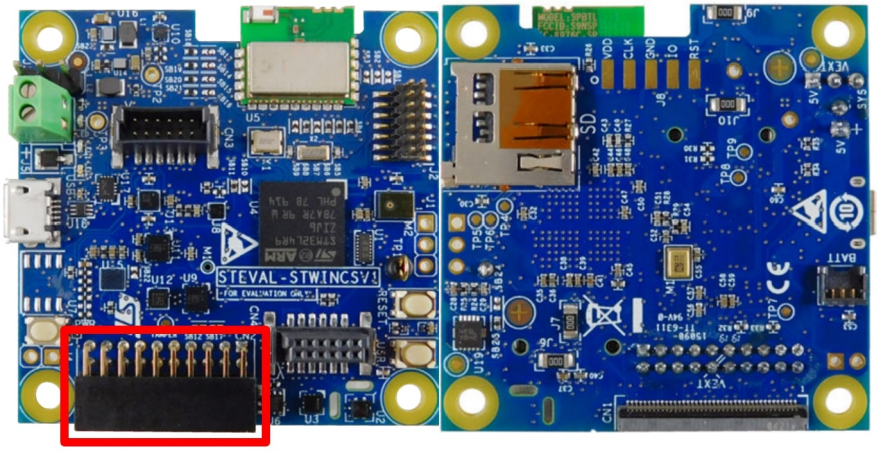

Figure 2.2: STWIN Core System board top and bottom

The *SensorTile Wireless Industrial Node* (STWIN) cointains a core system board with different sensors and an ultra-low-power microcontroller for vibration analysis and high precision local temperature and environmental monitoring. Each sensors communicate with the e STM32L4R9ZIJ6 microcontroller via SPI or I2C communication protocols.

The STM32L4R9xx devices are an ultra-low-power microcontrollers family (STM32L4+ Series MCU) based on the high performance Arm Cortex-M4 32-bit. The Cortex-M4 core cointains a single-precision floating-point unit (FPU), which supports all the Arm single-precision data-processing instructions and also implements a full set of DSP (digital signal processing) instructions and a memory protection unit (MPU), which enhances application security. These devices offer a fast 12-bit ADC (5 Msps), two comparators, two operational amplifiers, two DAC channels, an internal voltage reference buffer, a low-power RTC, two general-purpose 32-bit timer, two 16-bit PWM timers for motor control, seven general-purpose 16-bit timers, and two 16-bit low-power timers. They also include standard and advanced communication interfaces such as: I2Cs, SPIs, USARTs, UARTs, SDMMC, USB OTG full-speed. The STM32L4R9ZIJ6 operates from a 1.71 to 3.6 V for V_{DD}.

Several sensors are already mounted on the STWIN and they are able to communicate with the microcontroller. Some of them are listed below:

- HTS221 humidity and temperature sensor: an ultra-compact relative humidity and temperature sensor with a sensing element, which consists of a planar capacitor with a polymer dielectric capable of detecting changes in humidity. A dedicated ST process is required for the fabrication.

- LPS22HH MEMS pressure sensor: a piezoresistive pressure sensor which works like a barometer. The absolute pressure is detected by a sensing element, which consist of a floating membrane developed by ST.
- ISM330DHCX iNEMO IMU 3D Acc + 3D Gyro: a system-in-package. The sensing elements of the both sensors are deployed on the same silicon die, to obtain more robustness and stability.
- IIS2DH ultra-low power 3-axis high-performance accelerometer: an accelometer with digital I2C/SPI serial interface standard.
- IIS2MDC 3-axis magnetometer: it is an ultra-low-power 3-axis digital magnetic sensor.

The STWIN core system board includes several power management features that allow very low power consumption in final applications. The main supply for the entire system is through a lithium ion polymer battery (3.7 V, 480 mAh) and the integrated battery charger (STBC02) with Vin [4.8 -5.5 V]. The use of the lithium ion polymer battery is always optional.
Therefore, the STWIN board can be powered with different sources:

- V_USB: through micro USB connector [5V]
- V_{IN}: through J5 connector [4.8-5.5 V].
- VBAT: lithium ion polymer battery (3.7 V, 480 mAh)

There are three different buttons: one programmable to interact with the system (USR button), the second allows the user to turn the entire system on and off (PWR button), and the last one to reset it (RESET button).
Several connectors are also mounted on this evaluation board to provide communication with other external sensors. The one that has been used to communicate with the Analog Device EVAL-ADPD4000Z-PPG, named STMOD+ connector, is highlighted in the Figure 2.2. It provides both I2C and SPI communication protocol, some GPIO ports and also an external voltage supply in the standard configuration. The latter can be equal to 5 V or 3.3 V depending on how the board is powered,whether battery (VBAT) or USB connector (5 V) or J5 connector (5 V).
Once processed, data can be stored on a microSD card. A dedicated card socket is always accessible and a 4-bit wide SDIO port is available to access to the card and to achieve maximum performance.
Moreover, a Bluetooth module can be used to communicate with the external environment. Lastly, a Wi-Fi expansion, not included in the kit, can be plugged into the STWIN core system board.
A standalone debugging and programming mini probe for STM32 microcontrollers, named STLINK-V3MINI, allows the debugging and embedding process of the firmware through a JTAG/SWD interfaces for communication [35].

2.1.2 EVAL-ADPD4000Z-PPG

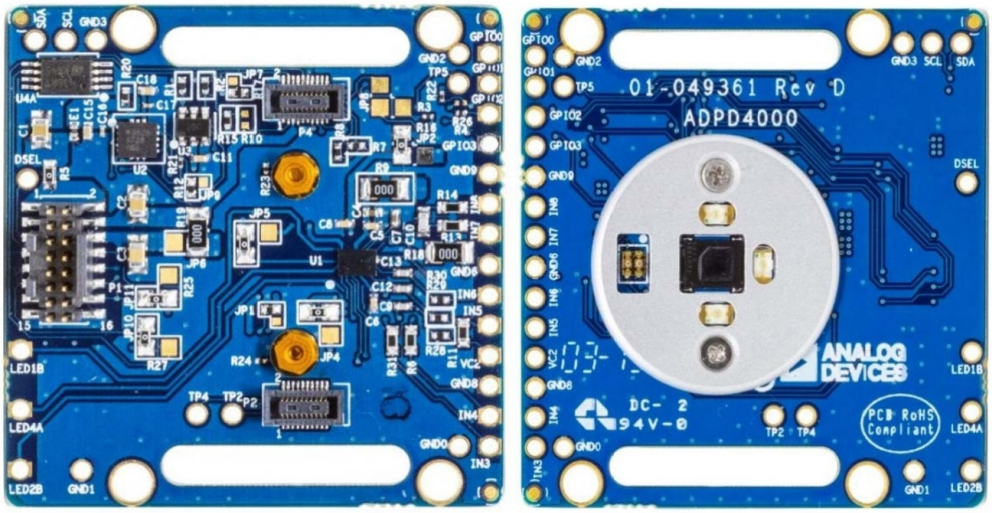

Figure 2.3: Top and Bottom side of the EVAL-ADPD4000Z-PPG

Several multiparameter systems that combine two or more measurement are available on the market. However, in most cases, a customized front-end is used to each measurements, hence a redundant building blocks are present. This is not suitable for a wearable system. The ADPD4000 family of biomedical front ends, by Analog Device (AD), is filling this gap in the market.
Two identical receive channels compose the front-end. They are differentially built, can be sampled simultaneously and each of them makes possible either a single-ended or differential measuring mode [36].
The device allows several measurements like Photoplethysmography (PPG), ECG, EDA, impedance, and temperature. The analog front end (AFE) consist of a transimpedance amplifier(TIA) with programmable gain, band-pass filter (BPA) with a high-pass corner at 100 kHz and a low-pass cutoff frequency of 390 kHz and an integrator capable of integrating ±7.5 pC per sample. Each channel is time multiplexed into a 14-bit ADC.
The digital block enables several operating modes, programmable timing, four general-purpose input/output (GPIO) pins, which can be used as interrupt or to provide external clock, block averaging, etc.
The entire system use a 1.8 V (1.7 - 1.9 V) analog core and 1.8 V/3.3 V compatible digital input/output (I/O).
A stimulus is provided by the central system to sensors connected to the device input and the response is evaluated, the information is stored in discrete data locations. Data can be accessed either by reading registers or through the FIFO (First in, First out) buffer. This highly integrated system includes an analog signal processing block, digital signal processing block, an SPI port, programmable pulsed LED current sources, and pulsed voltage sources for sensors that require voltage excitation [37]

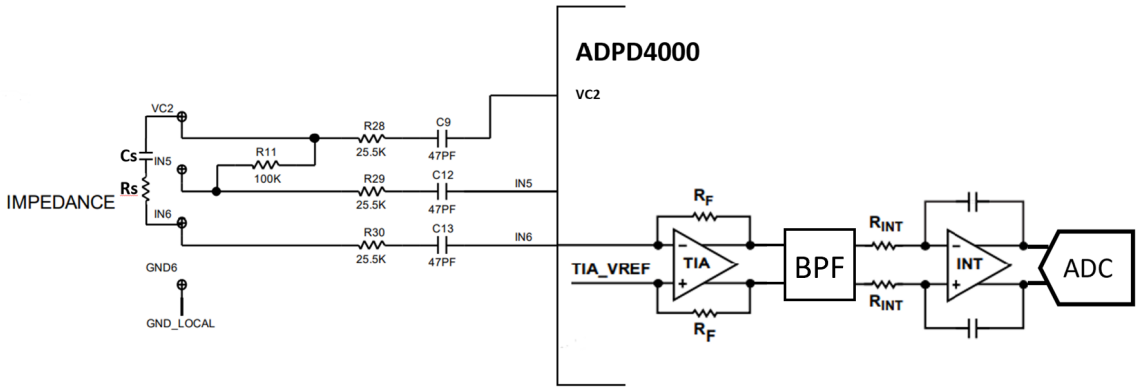

Figure 2.4: Analog Input for impedance measurements, single-ended configuration

.

In the following work, the ADPD4000 is used to measure the impedance variations due to a patch sensor and its contact with the skin. The VC2 and IN6 pins are used to connect the sensor in a single-ended configuration. Also a double-ended configuration is allowed by connecting the sensor to the IN5-IN6 pins, this could reduce noisy components. Once signal is sampled by ADC, it is possible to calculate the current at the input of the TIA amplifier using the formula below:

$$I = (\frac{0.92fC}{LSB}) * (MeasuredADCcodes - 8196) * (\frac{1}{0.81}) * (\frac{R_{int}}{2R_f}) * (\frac{1}{t_{pw}}) \qquad (2.1)$$

where fC refers to $femtoCoulomb$, R_{int} to is the series resistor to the input of the integrator, R_f is the TIA feedback resistor, t_{pw} refers to the width of a single pulse of the excitation train and 0.81 factor is the BFP gain.
The impedence is then evaluated by the formula:

$$Z = \frac{V}{I} \qquad (2.2)$$

where the excitation voltage of the ADPD4000, according to the datasheet, is typically 250 mV. Anyway, this value has been confirmed with the use of an oscilloscope placing the probe in the test point.

2.1.3 Boards Connection

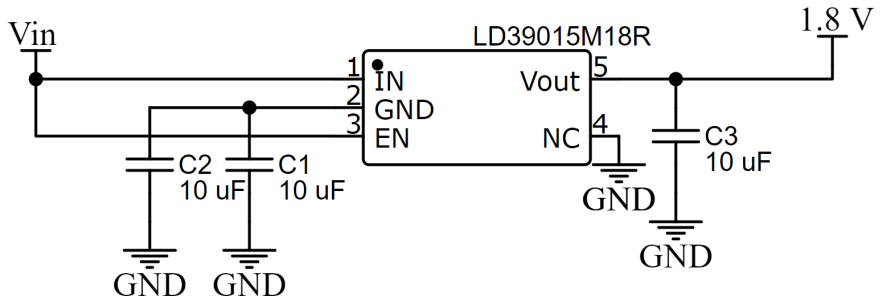

Figure 2.5: Voltage regulator application circuit

The STWIN and the AD board are connected on one side with STMOD connector and on the other with a pin header dedicated on AD board. As mentioned before, the ADPD4000 needs a voltage supply of 1.8V, but the external voltage provided by STWIN through STMOD connector is 5 V or 3.7 V, depending on how the board is powered.
First of all, the external voltage supply provided by STWIN is definitely turned down to 3.3 V, by connecting with a cable the TP3 pin (3,3 V), on the bottom side of the board, with the pin dedicated to the external power supply (Vext) available on J3 connector.
Consequently, to achieve the desired power supply a LD39015M18R low quiescent current and low noise voltage regulator is used, a device suitable for low power battery powered applications. It guarantees 150 mA output current and a typical dropout voltage of 80 mV.[38]
Voltage regulators work efficiently when a clean DC signal is fed into it, so two capacitor of 10 μF to the input and one of 10 μF to the output are used. Essentially, they act to short the AC noise of the voltage signal to ground, and filter only the DC voltage into the regulator.
The created design is shown in Figure 2.5.

To prevent digital logic control issues, the system must ensure that the output high (V_{OH}) logic output is higher than the input high (V_{IH}) logic input that it is controlling. According to the datasheet of STM32L4R9ZIJ6 microcontroller, the (V_{IH}) is 2.3 V, so the input/output voltage (VDDIO) of the ADPD4000 is set to 3.3 V, through the use of JP2 jumper present on the AD board.
The previous change leads to other several hardware issues.

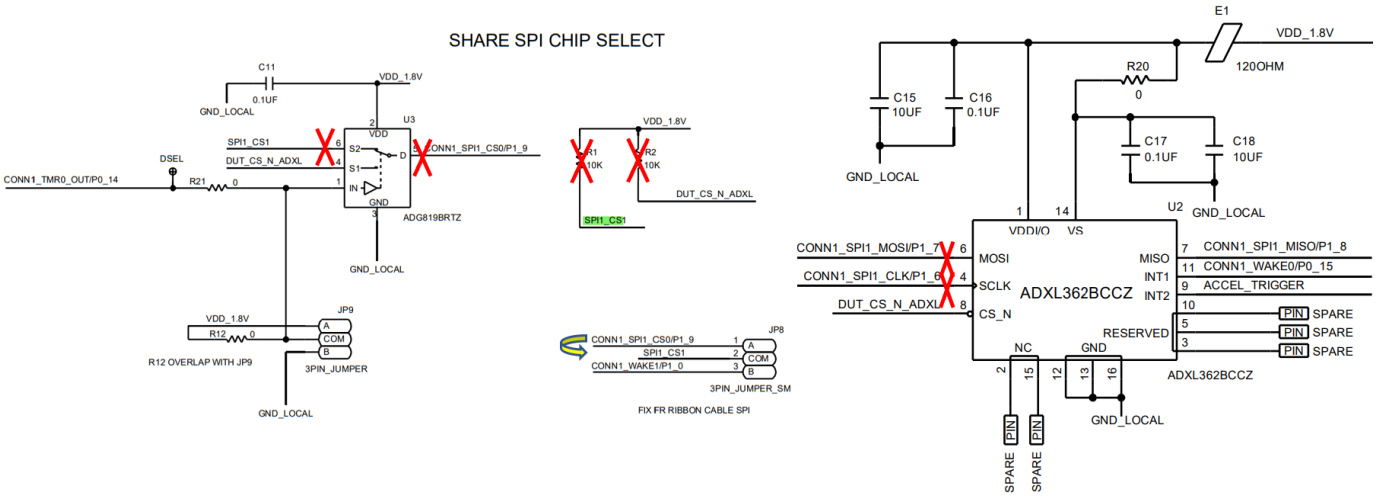

Figure 2.6: Chip Select module and Accelerometer on the ADPD4000 and respective changes

It happens that the power supply of the AD board shifts to an higher value, typically 2.4 V, leading to to a bad configuration registers writing.
This occurs because some module on the evaluation board do not allow the use of a VDDIO equal to 3.3 V. As Figure 2.6 shows, the ADXL362BCCZ accelerometer have a VDDIO equal to 1.8 V, therefore the lines related to the SPI work with that type of input/output supply, differently from the one desired. This leads to an increases in the power supply. The same problem occurs on the chip select module. For this reason, some conductive tracks on the PCB have been interrupted with the help of a viewfinder. Specifically, the following changes have been disrupted:

- CONN1_SPI1_CS0/P1_9 and SPI1_CS1 of the chip select module. These are connected via the connector JP8.
- CONN1_SPI1_MOSI/P1_7 and CONN1_SPI1_CLK/P1_6 of the accelerometer.

Moreover, also the R1 resistor have been removed because it pull up the SPI1_CS1 pin to a voltage equal to 1.8 V.
A summary of the changes operated on the board is shown in Figure 2.6. These have not limited the use of the board in any way.

2.1.4 Polyurethane patch Sensor

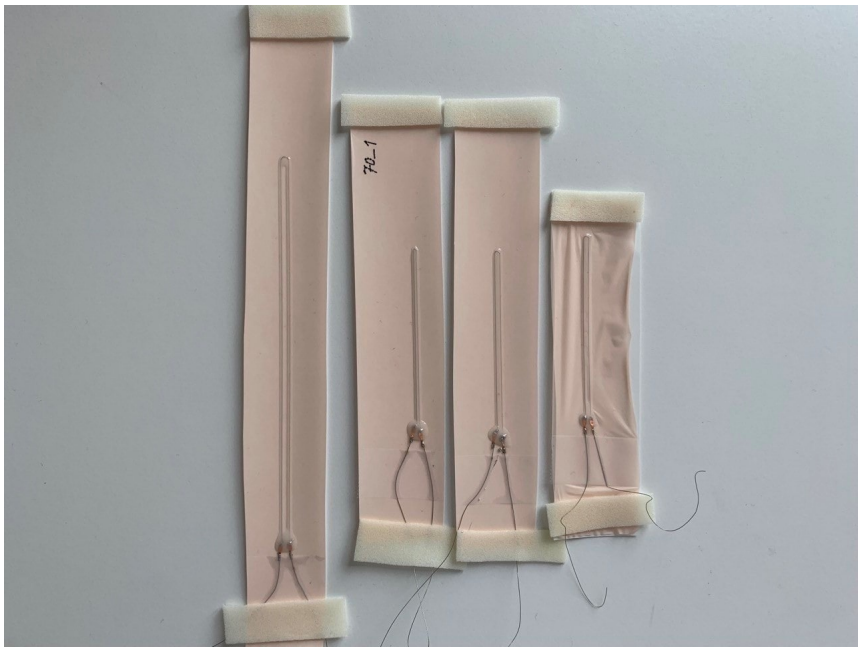

Figure 2.7: Several polyurethane patch sensor with different lenght

The stretchable sensors used are developed with the University of Uppsala, Sweden. The samples are fabricated using soft digital printed circuit board technology. This is based on direct ink writing of eutectic low-melting-point liquid metal alloy Galinstan® (Geratherm Medical AG, Germany). Galinstan is patterned onto 15 m thin, soft and stretchable polyurethane film inspire® 2331 (TC Transcontinental, UK) using a deposition setup consisting of tabletop robot MYT50L (Mycronic AB, Sweden) including three-axis movement with a resolution of 0.01 mm, high-precision benchtop fluid dispensing pressure controller and digital microscope monitoring and capturing the quality of the deposition process.
Conductive patterns are then encapsulated by dispensing of solvent-based silicone dispersion that cures at room temperature or elevated temperature by reaction with air humidity to a flexible and elastically deformable silicone coating.
Copper electrodes, with a thickness of 25 m and designed to prevent mechanical failure at the connector-liquid alloy interface, are used to facilitate connection with the measurement unit.
This encapsulant is not adhesive to the skin, therefore the sensor is attached first on an elastic patch and then to the skin through adhesive film. The adhesion of this to the skin is an important factor in measuring a good signal.
Several sensor have been designed with similar pattern: two lines connected by an arc. The difference between these pattern is the length of the lines and the distance between them. Specifically, the patch with a length of 70 mm and a line interval of 0.5 mm has been characterized to extract the properties and characteristics through 10 stress tests, in particular the sensor was stretched up to 22% with 2 mm intervals.

The total length of the conductive line considered is about 143 mm and the input resistance and capacity measured with a digital multimeter are equal to 6.8 Ω and 19 nF.
The following parameters are extracted evaluating the resistance changes:

- Linearity: it refers to changes in strength related proportionally to changes in strain. A good sensor would have a high and constant resistance variation over the strain range [39]. The R^2 value (coefficent of determination) is used to indicate how well a line of best fit represents the data it is fitted to.

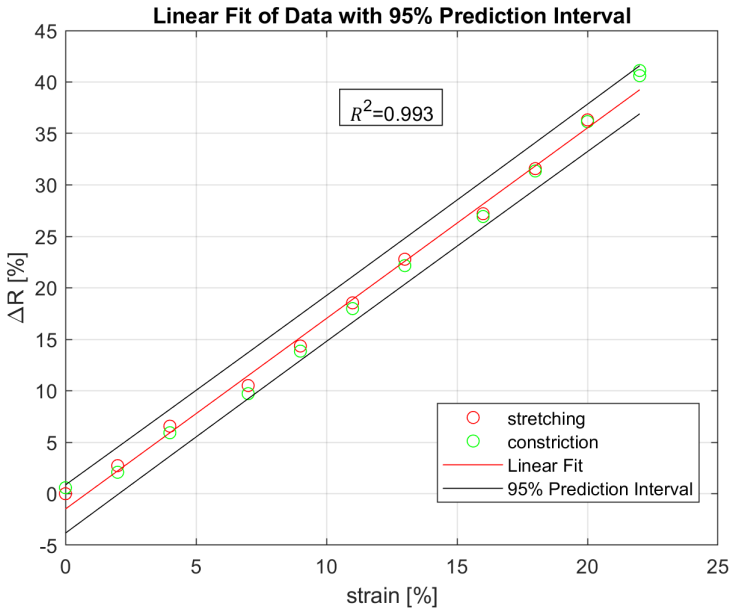

Figure 2.8: Resistance changes related to sensor stress of the polyurethene patch

- Sensitivity: this parameter is evaluated measuring the *Gauge Factor* (GF):

$$GF = \frac{\frac{\Delta R}{R}}{\frac{\Delta l}{l}} = \frac{\frac{\Delta R}{R}}{\varepsilon} \tag{2.3}$$

where R refers to the unstretched resistance defined as:

$$R = \frac{\rho * L}{S} \tag{2.4}$$

The GF is unitless and is calculated by taking the gradient of the best-fit line on the stress-strain variation plot. The GF of the sensor evaluated is equal to 1.85, similar to a metallic strain sensor ones. The higher the GF, the greater the resistance variations related with stress variations

- Hysteresis: it is the difference between the resistance measured during the loading cycle and the resistance at that same strain during the unloading cycle. The closer the values measured during the stress and non-stress phase, the greater the hysteresis. Figure 2.9 shows that the sensor used have a low hysteresis.

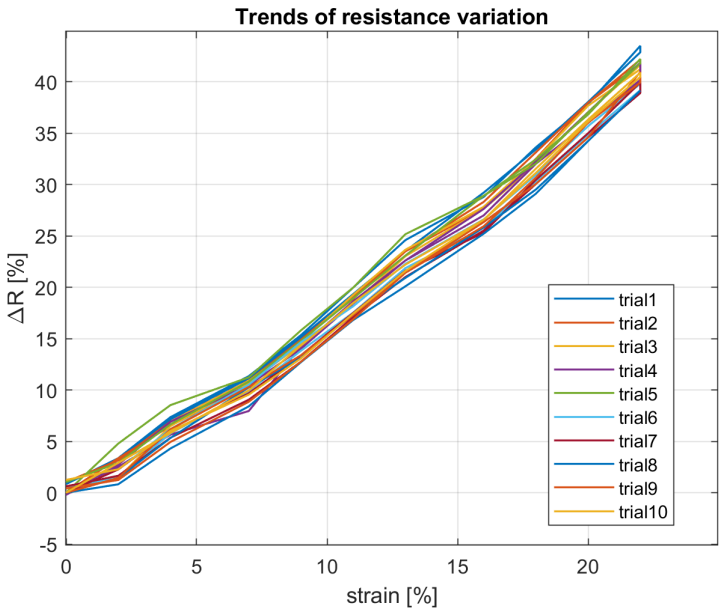

Figure 2.9: Hysteresis evaluation of the polyurethene patch

Similar behaviour has been obtained also with the patch sensors with different lenght.
Finally, it can be assumed that the sensor, within the range in which it has been stressed, exhibits good linearity, sensitivity and hysteresis.

2.1.5 Pulse Sensor

The Pulse is a wearable and non-invasive device, developed by STMicroelectronics, used for telemedicine purpose. In detail, it allows heart and breathing rate monitoring and at the same time detects physical activity and body posture.The device is connected to a disposable patch, which is attached to the chest. The patch includes four electrodes, two of them are used to inject an alternating current of 100 μA with a frequency of 50 kHz, the other 2 are used to measure the voltage, with which one lead ECG signal and 2 bioimpedance signals (DC and AC components) are acquired.

Figure 2.10: The Pulse device

In particular, the following parameters are extracted from the ECG signal[40] :

- Heart Rate;
- RR peak variability;
- Heart Rate variability;
- Electrode detachment alert.

Breathing rate is instead extracted from the bioimpedance signal. This is due to a change in voltage caused by a variation of lung air content to an externally applied electric current. Body posture and activity level are also detected with an accelerometer. Once acquired and processed, the device trasmits the extracted parameters and the recorded raw signals via Bluetooth to a computer, smartphone or tablet. Specifically, digital signal processing and real time elaboration are performed d with a low-power microcontroller of the STM32 family.
The entire system is shown in Figure 2.10. Three LEDs can be identified:

- The LED on the left refers to the battery status(the battery is rechargeable);
- The LED on the right provide alarms to the user. When it flashes, it means that the acquired signal is not reliable or the Bluetooth connection is not available;

- The central LED indicates the acquisition mode. If the light is fixed, the device is waiting for external commands (engaged mode). When the LED flashes quickly, the device is in streaming mode. When the LED flashes slowly, the device is in monitoring mode.

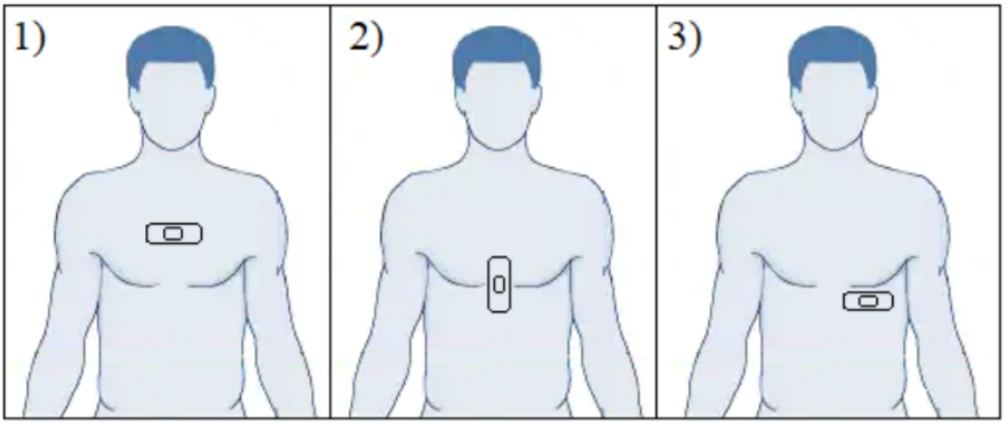

Figure 2.11: Several position of the Pulse sensor

Several position of the device could be used to o acquire reliable signals, Figure 2.11 shows the main ones.
Moreover, the Pulse device can operate in 4 acquisition modes:

1. **Power down mode**: the device is off;
2. **Engaged mode**: the device is visible and connectable to the remote unit via Bluetooth;
3. **Streaming Mode**: the device is powered ON and sends data, sampled according to the configuration settings, to the external device with a set periodicity;
4. **Monitoring mode**:The device is powered ON. It collects and stores data in the internal memory at the frequency defined in the configuration settings and send this data to the associated device.

2.2 Firmware Design

Several Integrated Development Environment (IDE) could be used to program the MCU. The STM32Cube IDE, for example, is the software owned by STMicroelectronics.
For this project, µVision®5 coming from Keil, property of ARM, has been utilized. A graphical tool, called STM32CubeMX software, is used to simplify programming and better manage time. It enables the user to easily configure an STM32 microcontroller and/or microprocessors and generates the initialization C code for the selected ARM® Cortex® -M core according to the chosen configuration. The following peripherals have been initialized on the STWIN side:

- SPI2 port: it allows the communication protocol to interface with ADPD4000 board.

- USART2: which enables the exchanging data with the PC. The data trasmission speed is 115200 bps. Data visualization is possible with the use of *Docklight*, a test, analysis and simulation tool for serial communication protocols via COM. It is possible to create a *.txt* file to save data.

- SDMMC: which provides a communication interface allowing the microcontroller to manage read and write operations with SD memory. Data bus widths of 4-bit mode is used for enhanced data throughput.

- TIM16: a timer with a resolution of 16 bit. It is used as interrupt to manage the data acquisition.

- TIM17: a timer with a resolution of 16 bit. It is used to display the timestamp and to monitor the sampling rate of data.

Regarding the EVAL-ADPD4000, the full AFE path is selected: TIA with 100 kΩ gain, a BPF with a high-pass corner at 100 kHz and a low-pass cutoff frequency of 390 kHz, and an integrator. Only one channel is used and a VC2 pulsing mode is selected. The IN6 pin is configure as single-ended input to evaluate impedance.
Operations of the ADPD4000 are controlled by an internal configurable controller that generates all the timing needed to generate sampling regions. The device provides up to 12 time slots for multisensor applications, but in this case only one time slot is selected. Specifically, each of them could include one or more modulation pulse. The higher the number of pulses, the higher the SNR of the signal. Also the width of the pulses can be selected.
The enabled time slot is repeated with a frequency of 300 Hz, it includes 11 pulses that repeat at a frequency of 50 kHz and have a duration of 3 μs. A graphical representation of the following configuration,obtained through the use of an oscilloscope, generated by the VC2 pin is shown in Figure 2.12.

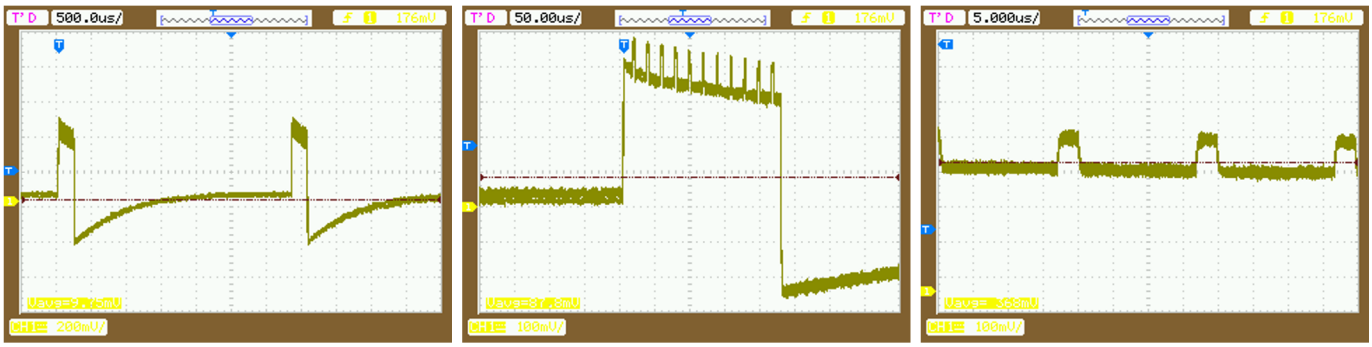

Figure 2.12: Timeslot frequency (300Hz), 11 pulses for each timeslot, pulse width and its frequency

2.2.1 Signal capture algorithm

The algorithm developed on µVision®5 performs data acquisition in *polling mode*. Specifically, after including all the necessary libraries, defining the variables and the private function prototypes, all the configured peripherals are initialized. Afterwards, battery and sd-card are configured. If something goes wrong, an orange LED starts blinking every 500 ms.
Once these operations are complete, the ADPD4000 configuration starts. First, the board recognition is done by reading the dedicated register, then all the adress configuration is loaded on the board. Thereafter, the two timers, TIM16 and TIM17, start and the program enters in the main while loop.
When the USR button is pressed, an interrupt is generated and the recording session starts. A green LED is turned on to confirm this step.
Moreover, at the same time, a file *.csv* is created and data will be saved in it.
Every 25 ms an other interrupt is generated by the TIM16 timer that allows impedance data and timestamp (provided by TIM17) reading.
At the end of acquisition, recording is concluded by pressing the USR button again.
A schematic view of the algorithm is presented in the flowchart below:

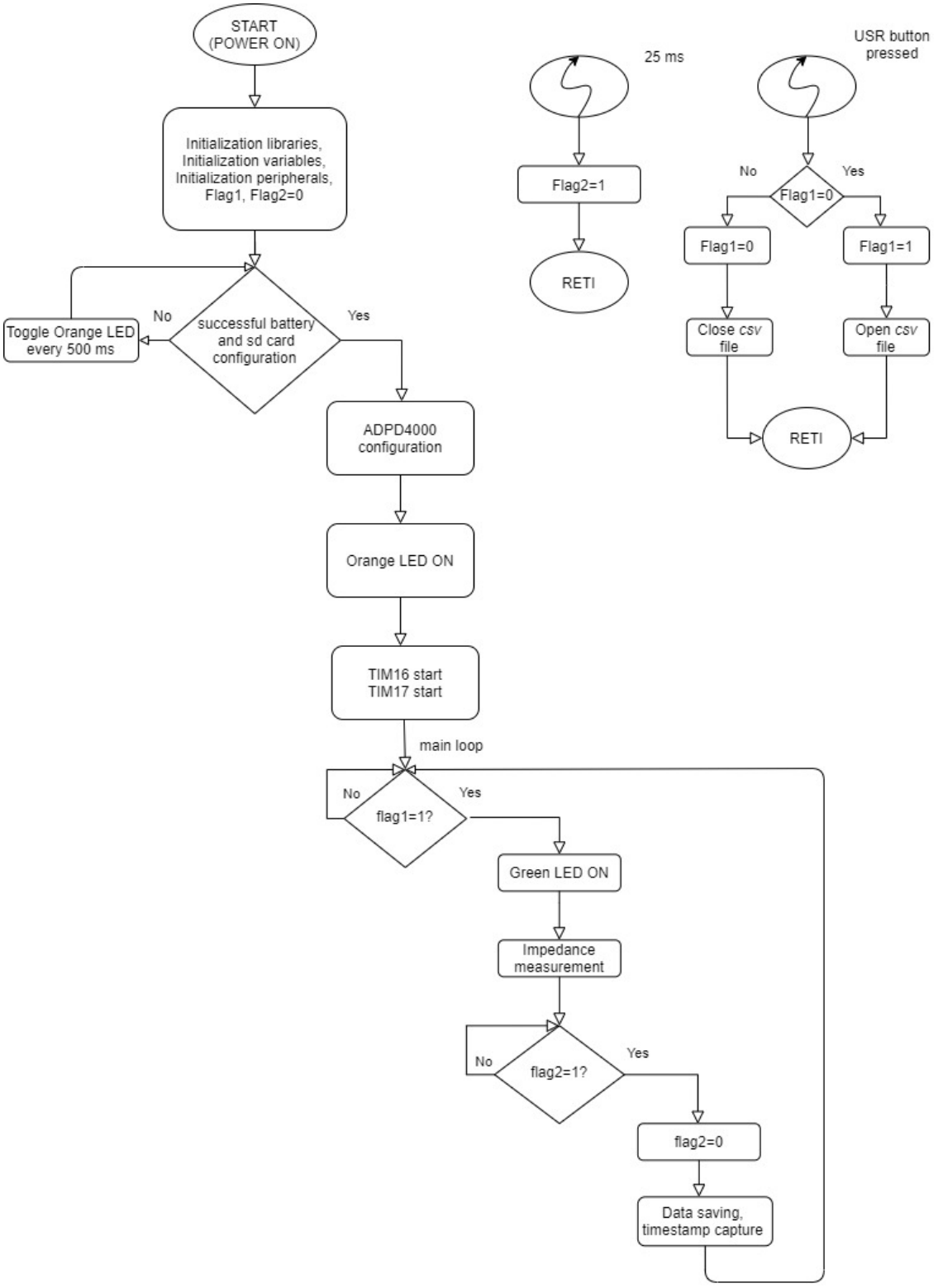

Figure 2.13: Main high level flowchart of the acquisition algorithm

2.2.2 SPI Protocol

SPI, Serial Peripheral Interface, indicates a serial communication system between a microcontroller and other integrated circuits, such as sensors, shift registers or ADCs, or between multiple microcontrollers.
SPI is a synchronous, full duplex master-slave-based interface. The information provided by the master or slave device is synchronized with the clock signal, either on the rising edge or the falling edge. Data exchange between the two or more devices can take place simultaneously.

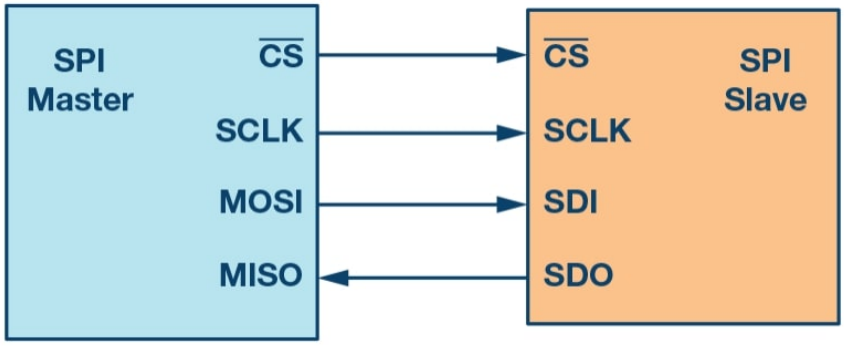

Figure 2.14: SPI configuration with master and a slave

The SPI interface can be either 3-wire or 4-wire.
The chosen configuration for the developed device focuses on the popular 4-wire SPI interface. The latter has the following four signals:

- Clock (SPI CLK, SCLK)
- Chip select (CS)
- Master out, slave in (MOSI)
- Master in, slave out (MISO)

In SPI protocol there is only one master and one or more slaves can be present and communicate with it.
Clock signal is generated by the master device. Data trasmitted between the master and the slave are synchronized to the clock generated by the first one.
Figure 2.14 shows the SPI connection between the two actors involved.
CS signal is used to select the slave. Specifically, when it is set to a low logical level the communication between master and slave is enabled. Instead, when it is set to a high logic level, the slave is disconnected from the SPI bus.
In the multi-slave configuration, one chip select signal can be used to drive all slaves, or a number of chip select signals equal to the number of slaves are required to control them individually.
The data is carried on MOSI and MISO lines. The former transmits data from the

master to the slave and the latter transmits data from the slave to the master.

In Summary, to start communication between master and slave, the former must

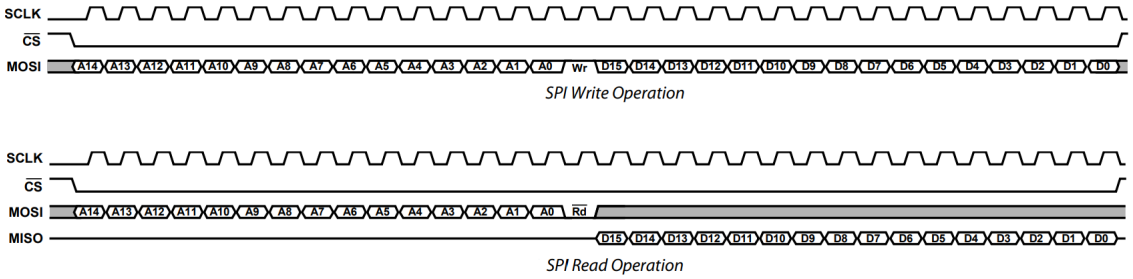

Figure 2.15: Read and Write operation of the ADPD4000

send the clock signal and the CS signal of the selected slave must be set to a low logic level. SPI is a full-duplex interface; both master and slave can send data at the same time via the MOSI and MISO lines respectively.

During SPI communication, the data is simultaneously transmitted (shifted out serially onto the MOSI/SDO bus) and received (the data on the bus (MISO/SDI) is sampled or read in). The SPI interface allows the user to select the rising or falling edge of the clock to sample and/or shift the data.

A detailed example of read and write operation of the ADPD4000 is shown in Figure 2.15: in the writing case, the MOSI sends first two bytes that contain the 15-bit register address and the last bit that specifies the type of operation requested. The register write occurs only when all 16 bits are shifted in prior to deassertion of the CS signal.

Instead, in the reading case, the MOSI likewise sends 15-bit that contain register address and the last bit that specifies the reading operation. The MISO responds with the information requested in the following 16 bits.

2.2.3 Power consumption

The power consumption of the entire system is measured by powering the STWIN with a benchtop power supply and connecting a multimeter in series with this. The current drawn by the system measured during the data acquisition stage is 57 mA. Considering that the current absorbed by unused peripherals is approximately 30 μA, it is possible to evaluate an estimated duration of the battery provided inside the STWIN kit with the formula below:

$$\Delta t = \frac{Q}{I} = \frac{480mAh}{(57 - 0.03)mA} = 8\ hours\ e\ 42\ minutes \tag{2.5}$$

where Q is the capacity of the Li-Po battery provided and I is the current consumed by the system during the recording session.

2.3 Calibration Tests

Before using the device to evaluate impedance, several calibration tests were performed to verify proper operation of the entire system.

2.3.1 ADPD4000 Calibration

The timing and amplitude of the pulses generated by ADPD4000, shown in Figure 2.12, are evaluated compairing the impedance measured by the ADPD4000 with the nominal impedance of the analog input (See the left side of the Figure 2.4). Several capacitances with orders of magnitude from pF to nF were placed at the input of the acquisition chain. How the device measures impedance has been discussed above, while the nominal impedance is obtained with the following formula:

$$Z = \sqrt{(\frac{1}{C9 + C13 + CS})^2 + (2R)^2} \tag{2.6}$$

The table below shows the results obtained:

C	**Znom (kΩ)**	**Z (kΩ)**	**|Znom-Z| (kΩ)**	**Err %**
22 pF	284.64	313.70	28.96	10.17
100 pF	174.88	177.60	2.71	1.55
1 nF	147.72	146.60	1.12	0.76
10 nF	145.03	143.32	1.71	1.18
100 nF	144.76	142.70	2.06	1.43

Table 2.1: Impedance values and relative errors with the chosen configuration.

As Table 2.1 shows, the percentage error for capacities in the order of tens of nanoFarads is very low, but is higher for capacities of a few tens of picoFarads. Specifically, the best performance is obtained for capacities in the order of a few nanoFarad. The resting capacitance of the polyurethane patch, measured by a bench test, is found to be in this range.

2.3.2 Frequency analysis

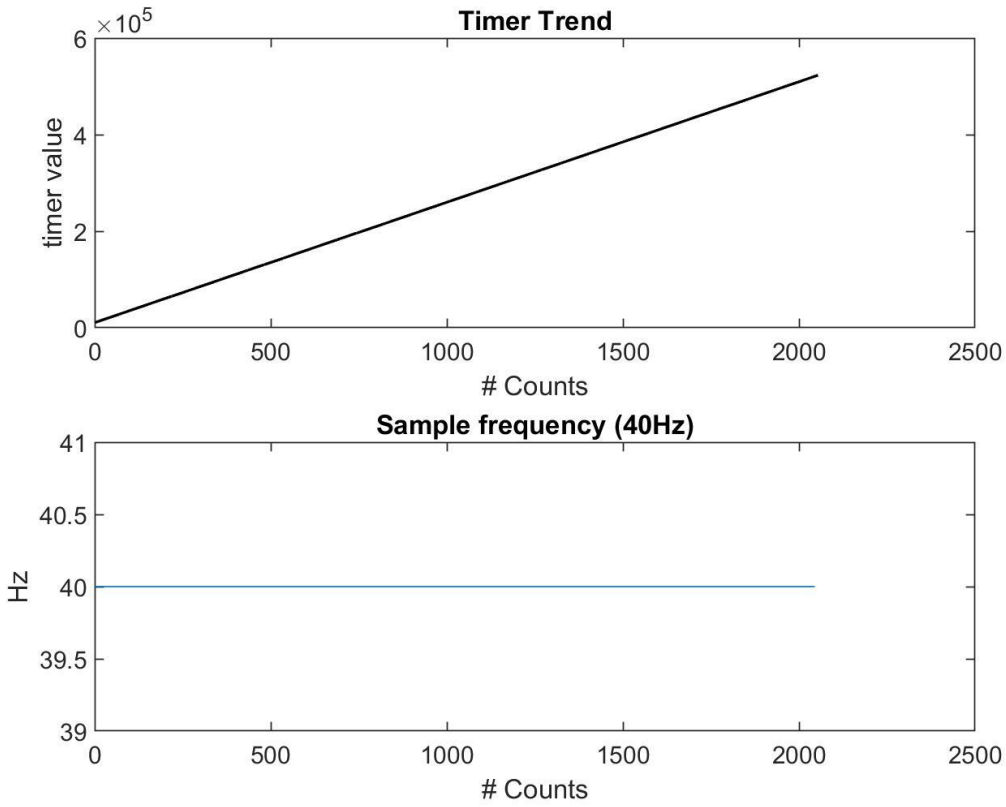

Figure 2.16: Timer trend and frequency check

The use of a timer allows data acquisition with high temporal accuracy.
Timing control is an important parameter that must be evaluated along with the integrity of the acquired data.
Once registered, timestamp values, provided by TIM17 and shown in Figure 2.16, are analyzed to verify data loss. As expected, the trend of the timer is increasing in accordance with the number of samples.
In addition, the chosen frequency of 40 Hz, supplied by the interrupt generated by TIM16, is verified by considering the difference between two sequential sample timestamps.
Specifically, the following formula is used:

$$fs_i = \frac{1}{x_{i+1} - x_i} \tag{2.7}$$

where x is the timestamp value.
Finally, there is no data loss during the entire acquisition process

2.4 Software Design

Once signal acquired and saved on the sd card, it is processed to extract its main information. The generated *.csv* file is easily loaded and analyzed within the Matlab2021a® environment.
This section illustrates the algorithms which have been employed for respiration signal and how vital parameters are derived from this.

2.4.1 Pre-Processing

Pre-processing steps are necessary to smooth and to eliminate unnecessary information from the entire signal. Firstly, the raw signal is loaded and plotted. If there are some outliers, they are removed with a Hampel filter, which defines an outlier as element more than three local scaled MAD (medial absolute deviation) from the local median over a specified window length.

Afterwards, the breathing signal is divided into 10 seconds windows and is filtered preserving the initial condition through the frames.
Finite impulse response (FIR) filters are used to reduce noisy components. Specifically, a low-pass 60 order filter with a cut-off frequency of 0.001 Hz is used to mitigate the DC component of the raw signals and a high-pass filter with the same order, but with a cut-off frequency of 1 Hz is used to attenuate the high frequency components.
The cut off frequencies have been chosen considering the bandwith of the signal, which is 0.06 Hz (corrisponding to 4 bpm) to 1 Hz (corrisponding to 60 bpm). Module and phase of the developed filters are shown in Figure 2.17.

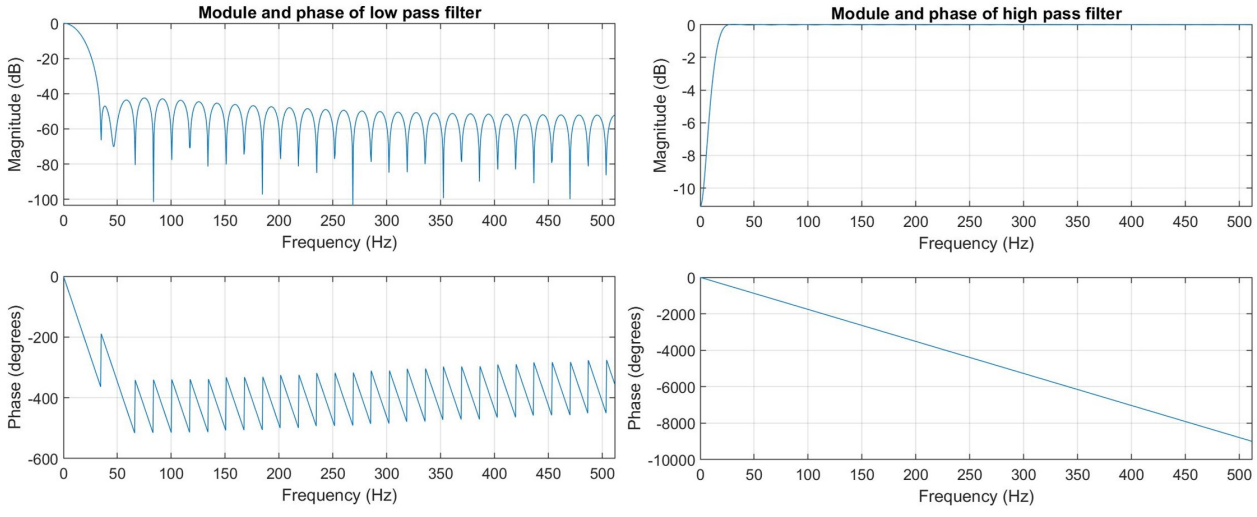

Figure 2.17: High and low pass filter module and phase

FIR filters with finite-duration impulse response, have both advantages and disadvantages compared to infinite-duration impulse response (IIR) filters. The main reasons to use them are:

- They can have exactly linear phase.
- They can be realized efficiently in hardware.
- They can be used in real time application
- They are always stable.

Anyway, also some disavantages have to be considered. One of the main disadvantages is that FIR filters generally require a much higher filtering order than IIR filters to achieve the same level of performance. Consequently, the delay introduced by these filters is greater than that of a IIR filter of equal performance. However, the latter has been recovered with a signal shift.

Additionally, a Savitzky-Golay finite impulse response (FIR) smoothing 2 order filter is applied to smooth the signal with a frame length of 2 seconds. This filter fit successive sub-sets of adjacent data points with a low-degree polynomial by the method of linear least squares. In general, filtering with Savitzy Sgolay filter consists of replacing each point of a signal by some combination of the signal values contained in a moving window centered at the point, on the assumption that nearby points measure nearly the same underlying value.

An example of complete filtered signal compared with raw signal is shown in Figure 2.18

Furthermore, the signal spectral estimation before and after pre-processing is reported in Figure 2.19. It is possible to notice that already from the unfiltered signal the power density in the considered band is predominant. Noisy components are attenuated after filtering.
An estimate of SNR after filtering can be made by measuring the ratio of signal to noise. Specifically, only noise due to electrical component is considered. Both signals, signal with noise and only noise, are filtered and the power density of them within the bandwidth considered [0.04-1 Hz] is measured.

$$SNR = 10log_{10}\frac{P_s}{P_n} = 40.2\,dB \tag{2.8}$$

where P_s and P_n are the power density of signal with noise and noise respectively.

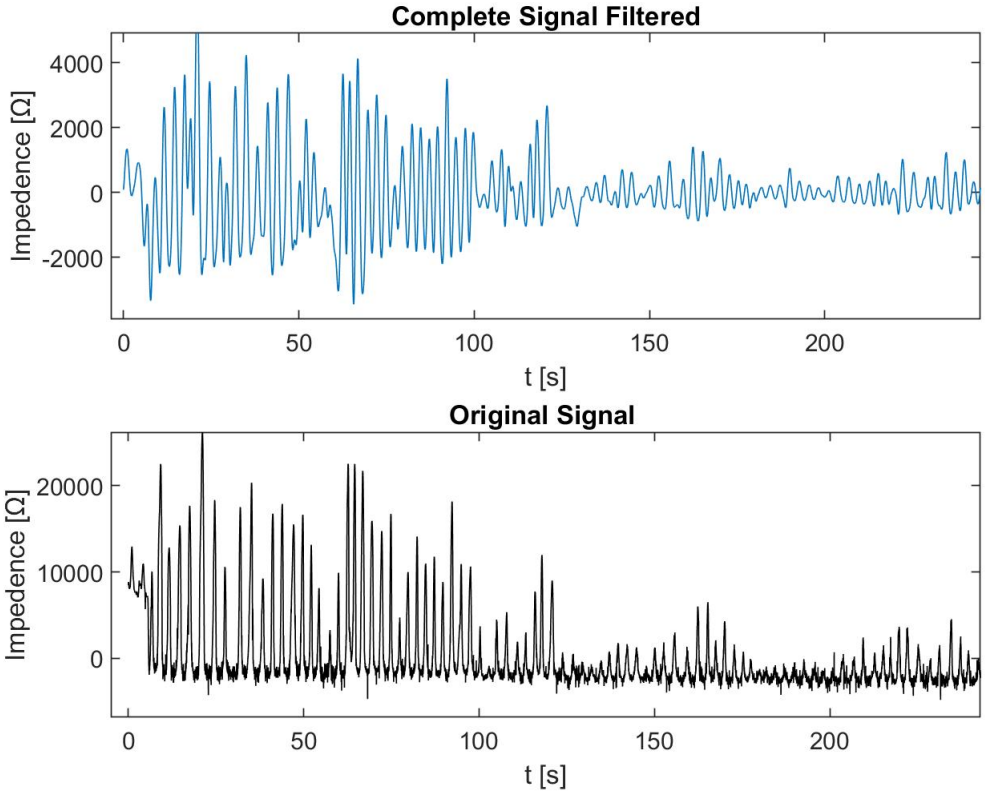

Figure 2.18: Comparison of raw and filtered signal

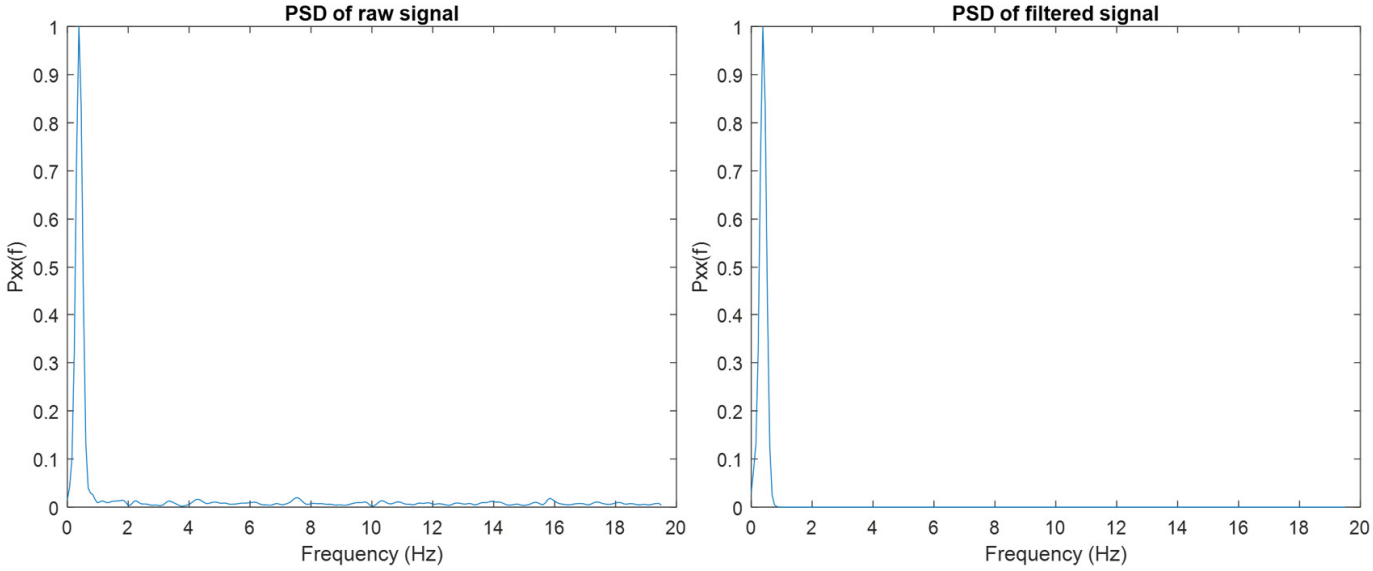

Figure 2.19: Power spectral density before and after filtering

2.4.2 The proposed algorithm

Several algorithms can be used to study respiratory signal and to extract RR from this. They can be in time domain, i.e. peak detection, autocorrelation, and frequency, i.e. AR model and FFT.
The algorithm developed in this work is in time domain. This is because embedding a time domain algorithm into a microcontroller results in less computational weight.

Once data has been cleaned with filtering steps, the entire signal is analyzed throught windows of 60 seconds size. Afterwards, all the peaks and troughs are identified according to the following principle:

$$peaks \qquad x_{i-1} < x_i > x_{i+1} \tag{2.9}$$

$$troughs \qquad x_{i-1} > x_i < x_{i+1} \tag{2.10}$$

The choosing of this methodology has made it possible to get away from the common threshold criteria, which can be ineffective in many cases.
At the same time, due to noise or motion artifact, many several false peaks and troughs are identidied by this first step. This is shown in Figure 2.20.
The following steps aim to solve the resulting problem.
Based on physiological conditions, it has been assumed that two peaks cannot be less than one second and half seconds apart. According to this consideration, peaks closer than one second and half to each other are identified and the higher of the two is chosen as the true peak and the second is removed. The same approach is applied on the troughs, the minimum of the minimums is chosen between the two nearest neighbors.
The advantages of this procedure is shown in Figure 2.21.
Nevertheless, a third step is also necessary to remove the other peaks and troughs due to noise. The following procedure has been followed: a peak is an absolute maximum if and only if the amplitude of all points of the signal in a radius of one second around it is less than its own. The same procedure is applied to the minimums.
The results obtained by this procedure are displayed in Figure 2.22.
Finally, sometimes, depending on the type of signal recorded, a fourth step is included to always get a peak and a trough in an alternating manner. In fact, it could be possible that two minimums are detected between two peaks or vice versa. In that case, the minimum value between the two is selected as final trough, or the maximum value as final peak.

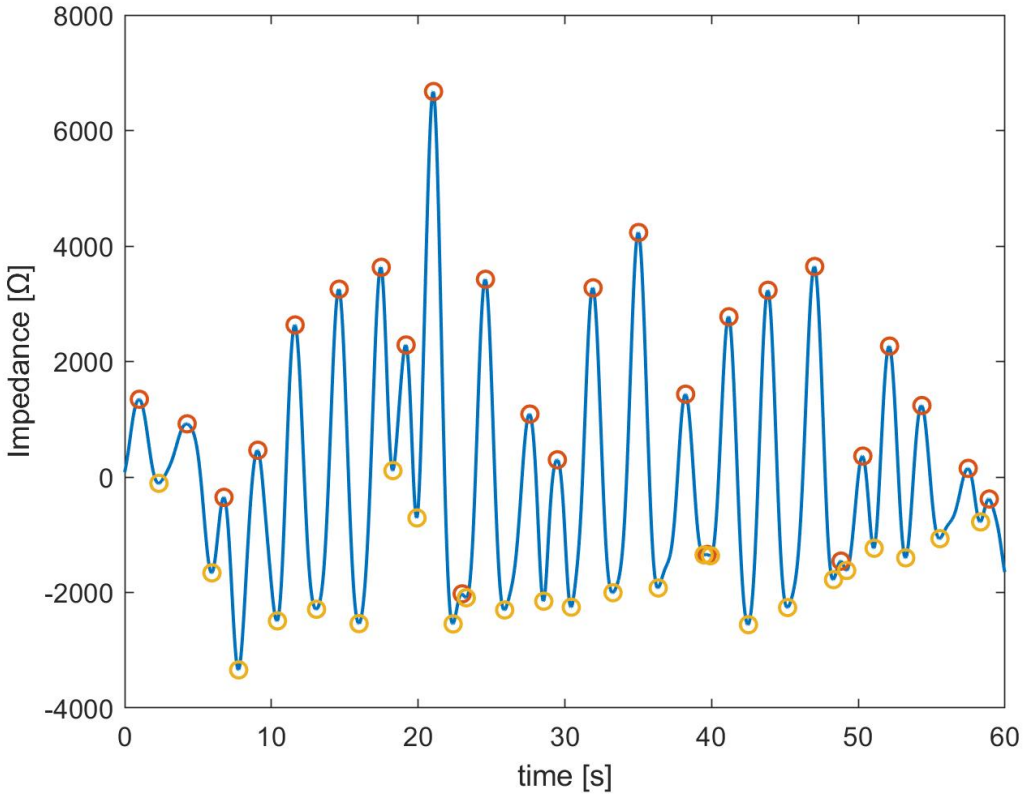

Figure 2.20: Peaks and troughs after the first step.

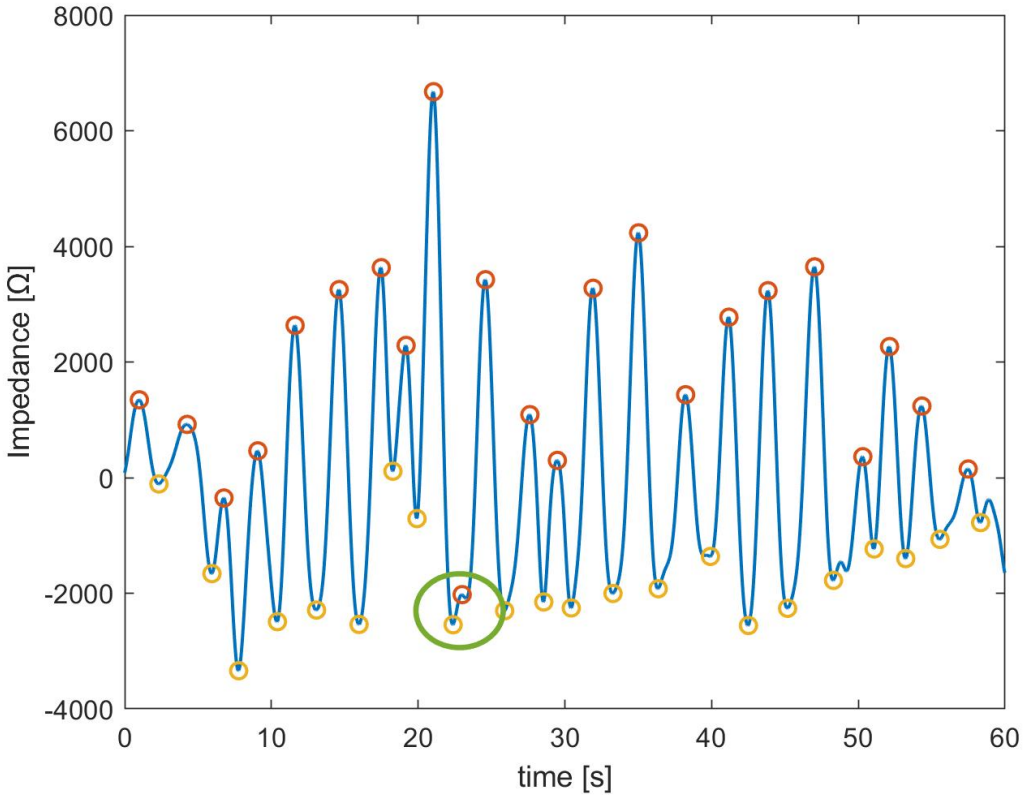

Figure 2.21: Peaks and troughs after the second step.

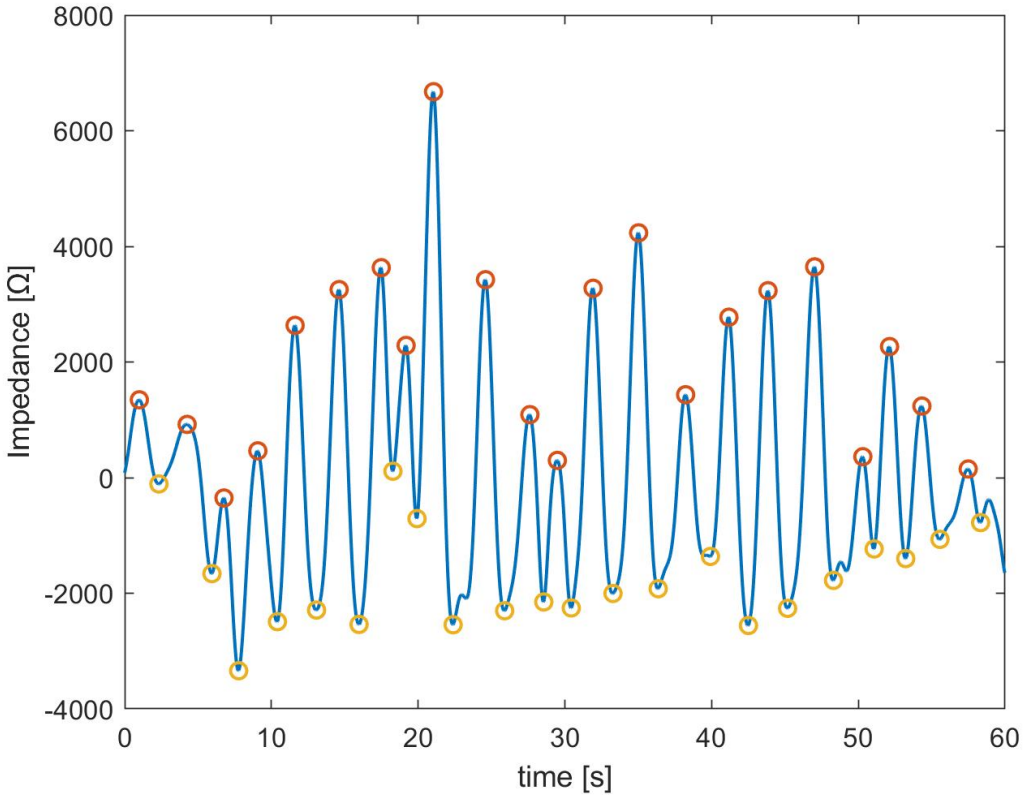

Figure 2.22: Peaks and troughs after the third step.

2.4.3 Feature Extraction

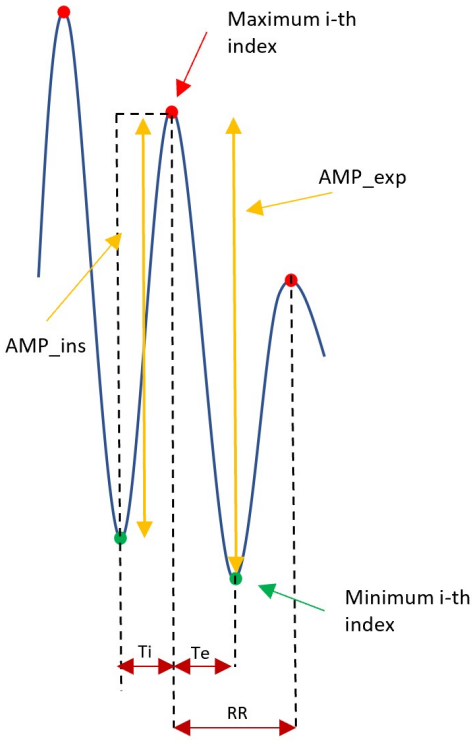

Figure 2.23: Main parameters extracted from respiration signal.

Once all the peaks and troughs definitely selected, it is possible to extract vital parameters from the respiratory signal.
Specifically, the following ones are analyzed in this work:

- **BR**: Breathing Rate, is obtained by counting the number of the peaks in each window;
- **RR**: It is defined as the mean distance among the peaks in each windows;
- **Ti**: Inspiratory time, it is obtain first considering if the first point in the window considered is a peaks or a trough. Afterward, if the first point is a trough, the parameter considered is defined as the time distance between this one and the following peak ;
- **Te**: Expiratory time, it is obtain first considering if the first point in the window considered is a peaks or a trough. Afterward, if the first point is a trough, the parameter considered is defined as the time distance between the following peak and the following trough ;
- **I/E**: Inhalation-exhalation time ratio, it refers to the ratio of the duration of inspiratory and expiratory phases. It represents a compromise between ventilation and oxygenation.

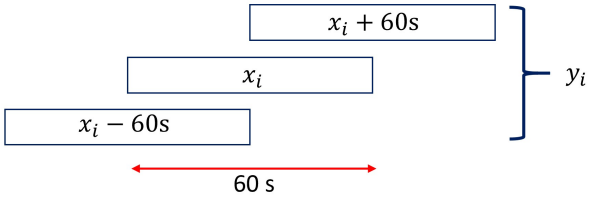

Figure 2.24: Moving average method to extract parameter.

For the purpose of not obtaining polarized results, a moving average method is applied considering consecutive windows of 60 seconds length. Specifically, each parameter is calculated in the current window and then averaged with the same parameter calculated in the next and previous window overlapped by 50%.

The same algorithms are applied on the signal proveded by the gold standard. It is possible to visualize bioimpedance signal registered thanks to a dedicated pc application that saves data on a *.txt* file. This is loaded on Matlab environment, processed and results are then compared to the one of the sensor.

2.4.4 Statistical Feature Extraction

In order to evaluate the performance of the algorithm developed, the parameters extracted both from polyurethane patch and Pulse sensor signal are compared with the listed metrics:

- Mean Absolute Error (MAE): it is an arithmetic average of the absolute errors

$$MAE = \frac{\sum_{i=1}^{N} |x_{ss} - y_{im}|}{N} = \frac{\sum_{i=1}^{N} |e_i|}{N} \tag{2.11}$$

  where x_{ss} and x_{im} will be used for polyurethane patch-derived and Pulse sensor parameters respectively. Specifically y_{im} is the Pulse and x_{ss} the polyurethane patch sensor extracted value. The mean absolute error uses the same scale as the data being measured.

- Standard Deviation (SD): which give an idea of how spread out the data is. It is a measure of how far each observed value is from the mean.

$$SD = \sqrt{\frac{\sum_{i=1}^{N} |x_i - \mu|}{N - 1}} \tag{2.12}$$

  where μ is the mean of x_i.

2.4.5 Flowchart of the Matlab algorithm developed

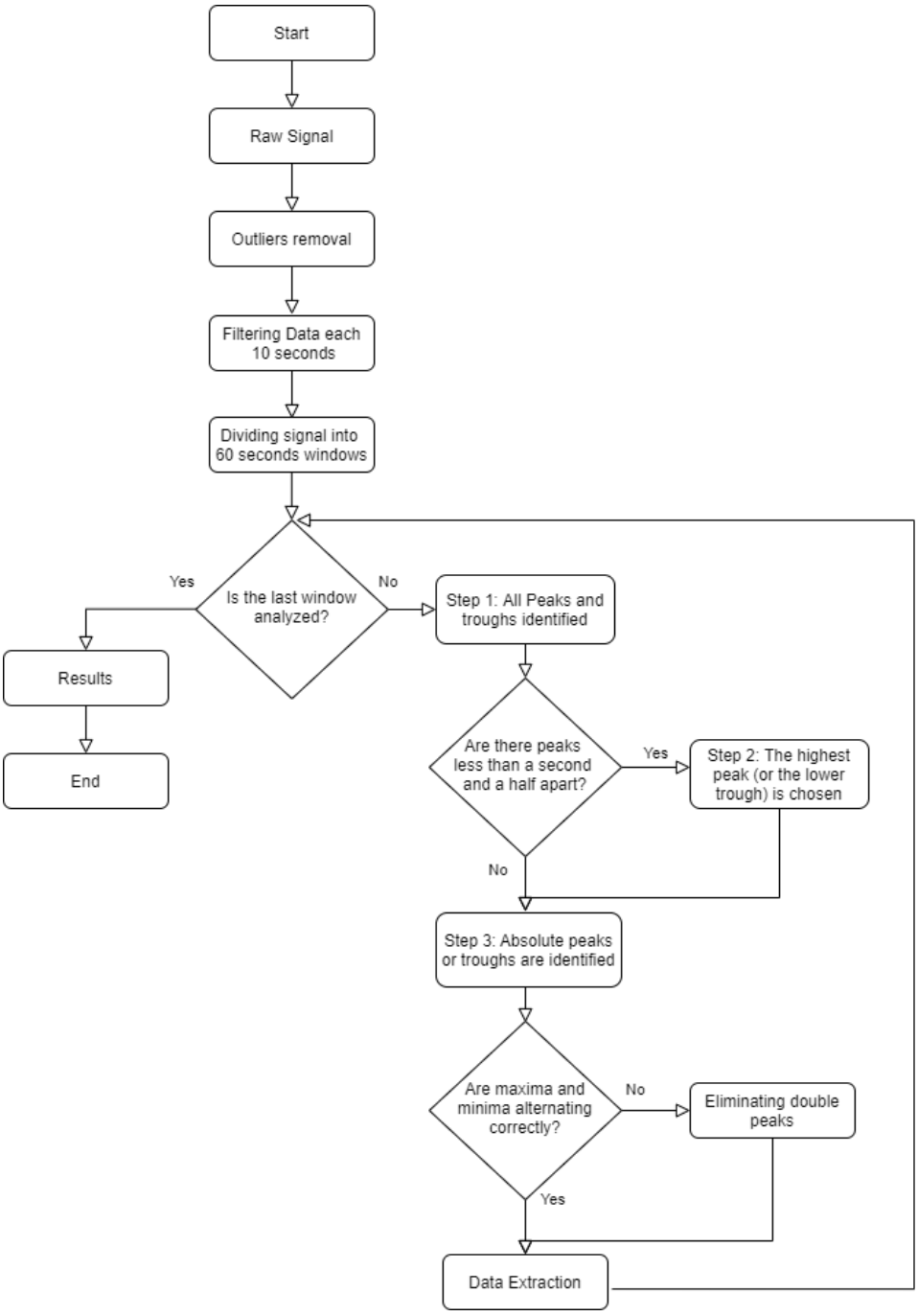

Figure 2.25: Main steps of matlab algorithm developed.

Chapter 3

Results

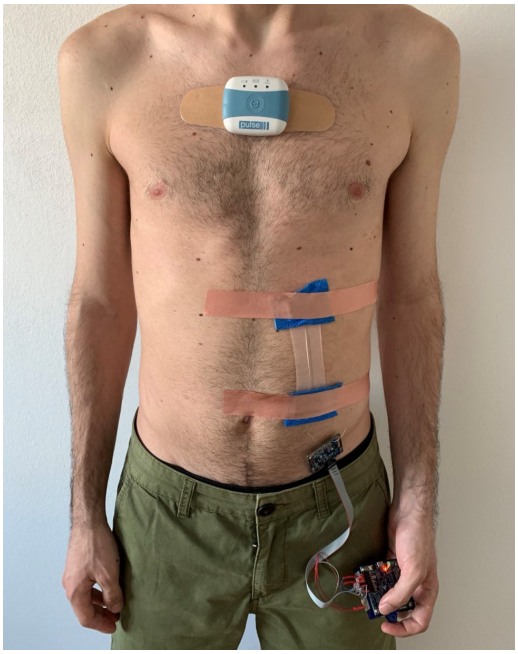

Figure 3.1: Complete system configuration

The system developed is designed as a short-term monitoring device. Impedance variations are assessed over time by continuously recording at a sampling rate of 40 Hz, respiratory rate data is subsequently stored.
Data collected by the device should be evaluated by healthcare professionals on a case-by-case basis.
In order to obtain the best possible signal quality, sensor positioning is an extremely important parameter that must be considered. According to the literature, the sensor should be placed at the last rib of the patient's body. If necessary, the area should be cleaned and shaved.
The Pulse device, used as gold standard, is also attached to the chest with the use of a disposable patch.
The complete configuration is shown in Figure 3.1.

3.1 Acquisition Protocol

Once the sensors are placed, the recording session starts.
The respiration signal is acquired in several and common body position in order to evaluate differences in impedance variation. Specifically, sitting, standing, and walking positions are considered. Each subject wearing the device has been required to perform the following protocol: 5 minutes sitting, 5 minutes standing, and 5 minutes walking consecutively without talking or laughing, in order to reduce noisy components.
Finally, parameters are extracted and the results are compared in the following paragraphs.

3.2 Polyurethane patch results

The wearable device developed is tested with several trials on different patients and the results of the signals acquired with the polyurethane patch and the Pulse device are compared. For each trial, all parameters presented are extracted, in order to define an overall performance of the implemented device.

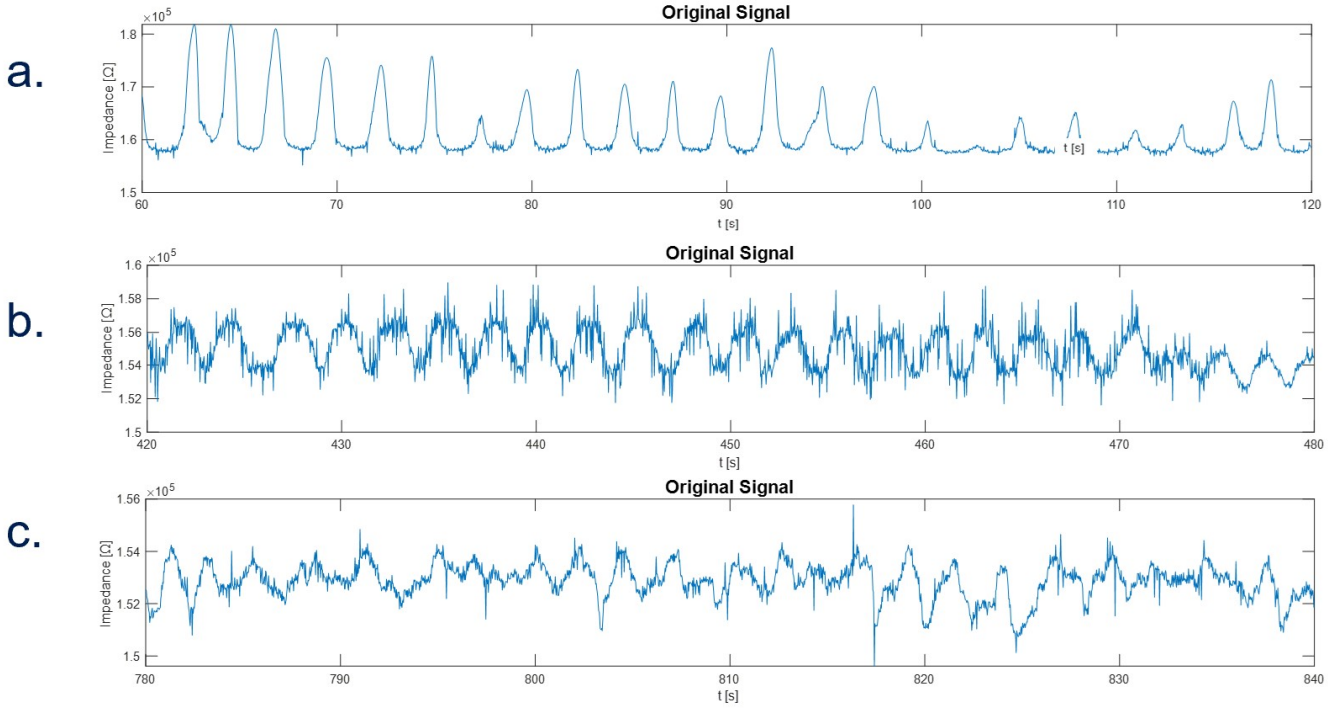

Figure 3.2: Examples of signals in different body positions.

First, because body posture could have a significant influence on lung volume and subsequent patterning of respiratory signals, the morphology of the recorded signals is analyzed.
Several remarks can be made by observing Figure 3.2. Specifically, signal **a** is a 60-second long signal window recorded during the sitting position. On the other hand, signals **b** and **c** refer to different windows recorded during standing and walking position respectively and in the same recording session as the first window. As expected, it can be notice as the signal **a** is less corrupted by noise componets than signal **c**. In the latter case, the respiratory signal is indeed less perceptible. The higher the noise, the less accurate will be the estimates of the parameters considered. Furthermore, several assumptions can also be carried out on the signal amplitude. In particular, the peak-to-peak amplitude of the respiration signal in sitting position is wider than the others. A variation of about 20 kΩ can be detected. This can be explained by the fact that in the sitting position changes in the geometry of the rib cage and abdomen are more relevant and the sensor is in better contact with the skin, so it follows skin deformations more accurately.

Based on these assumptions on morphology, the results obtained on the study of parameters extracted from the respiratory signal will be shown below. It has been chosen to show the trend of the parameters considered in the following way: first a summary table will show the results obtained for all the trials done, then the results of *Trial 1* acquisition will be shown to have a graphical view of the data.

3.2.1 BR results

Breathing Rate (BR) results comparison between gold standard device and patch sensor are shown below.

Trial	MAE ± SD [bpm]			
	BR	BR_sitting	BR_standing	BR_walking
1	0.93 ± 1.06	0.60 ± 0.84	1.14 ± 1.14	1.20 ± 1.30
2	0.40 ± 0.64	0.40 ± 0.89	0.40 ± 0.55	0.60 ± 0.55
3	1.87 ± 2.06	0.60 ± 0.84	2.00 ± 1.87	3.00 ± 2.00
4	0.86 ± 1.02	0.80 ± 1.10	0.80 ± 1.22	1.00 ± 0.71
5	1.00 ± 1.03	1.60 ± 0.89	0.60 ± 0.55	0.80 ± 1.00
6	1.53 ± 1.84	1.00 ± 1.30	1.20 ± 1.10	2.40 ± 1.87

Table 3.1: Breathing Rate error evaluation between patch sensor and gold standard.

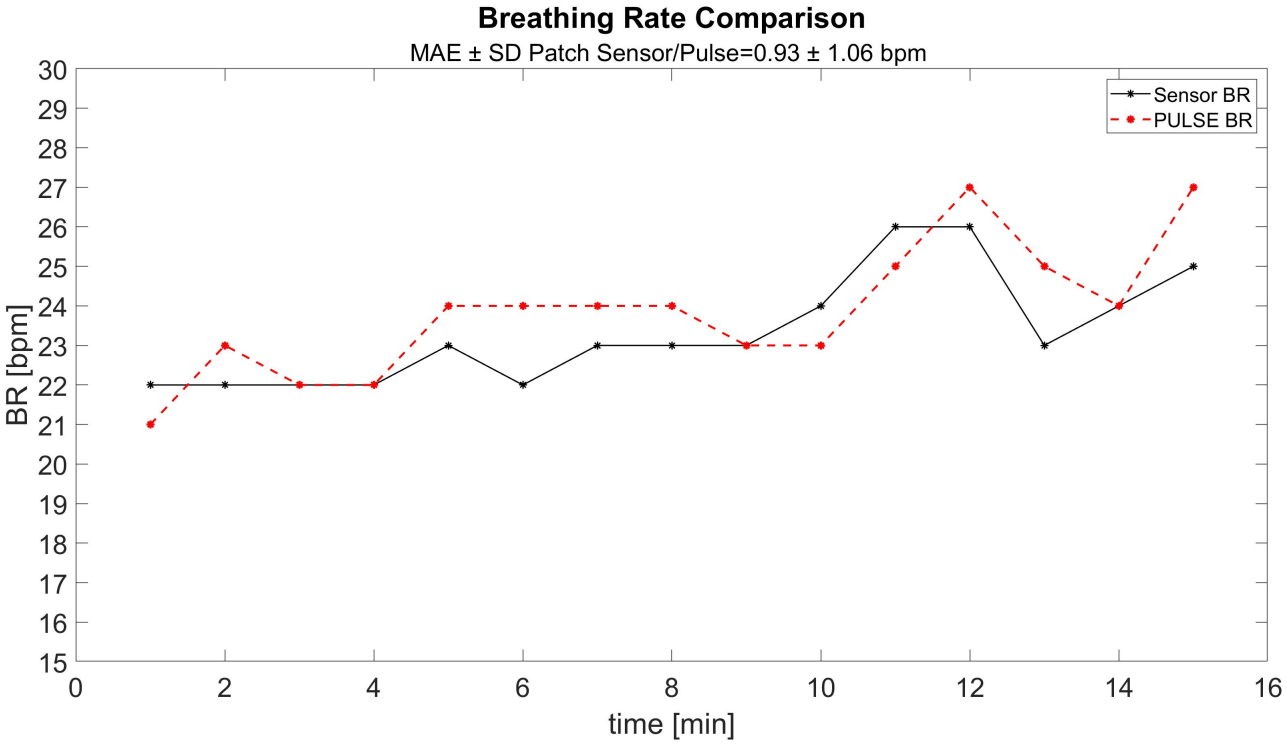

Figure 3.3: Brething rate comparison

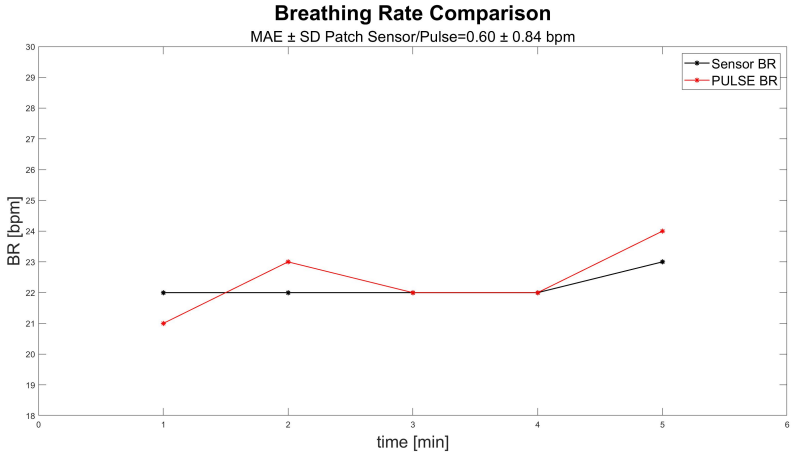

(a) *Sitting BR results comparison*

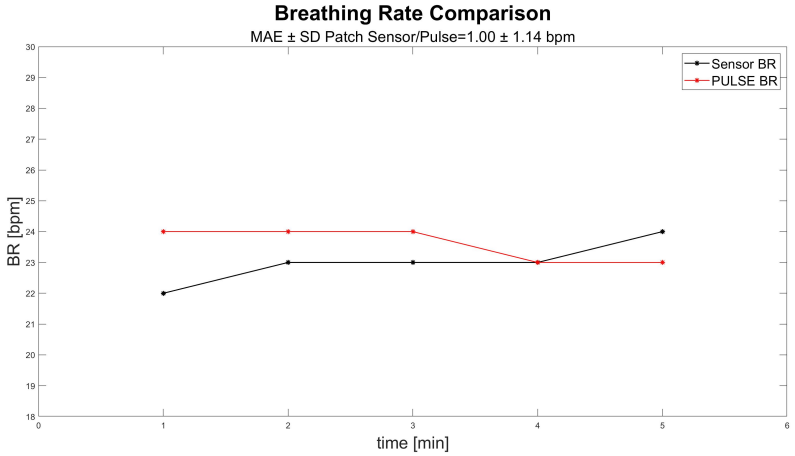

(b) *Standing BR results comparison*

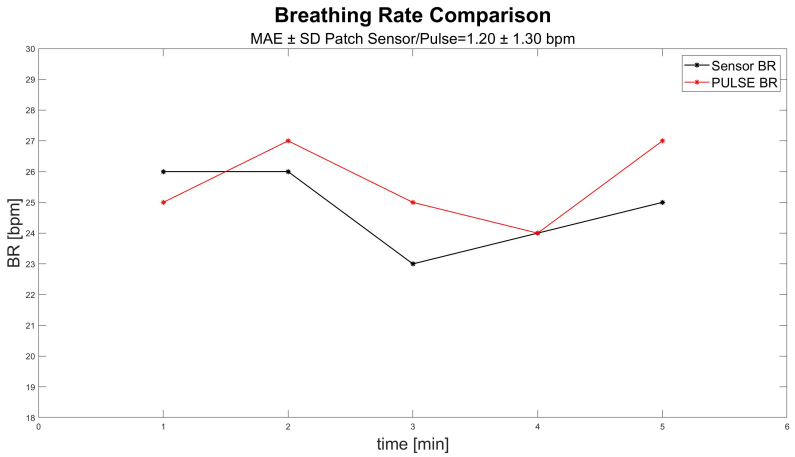

(c) *Walking BR results comparison*

Figure 3.4: Specifically comparison of BR results

3.2.2 RR Results

RR time results comparison between the two methods are presented in this paragraph.

Trial	MAE ± SD [bpm]			
	RR	RR_sitting	RR_standing	RR_walking
1	0.09 ± 0.11	0.06 ± 0.09	0.09 ± 0.11	0.12 ± 0.13
2	0.06 ± 0.08	0.06 ± 0.10	0.05 ± 0.06	0.07 ± 0.08
3	0.18 ± 0.19	0.06 ± 0.08	0.18 ± 0.18	0.30 ± 0.21
4	0.10 ± 0.12	0.08 ± 0.12	0.09 ± 0.11	0.09 ± 0.09
5	0.17 ± 0.18	0.35 ± 0.17	0.11 ± 0.10	0.05 ± 0.07
6	0.16 ± 0.21	0.10 ± 0.14	0.15 ± 0.16	0.22 ± 0.22

Table 3.2: RR time error evaluation between patch sensor and gold standard.

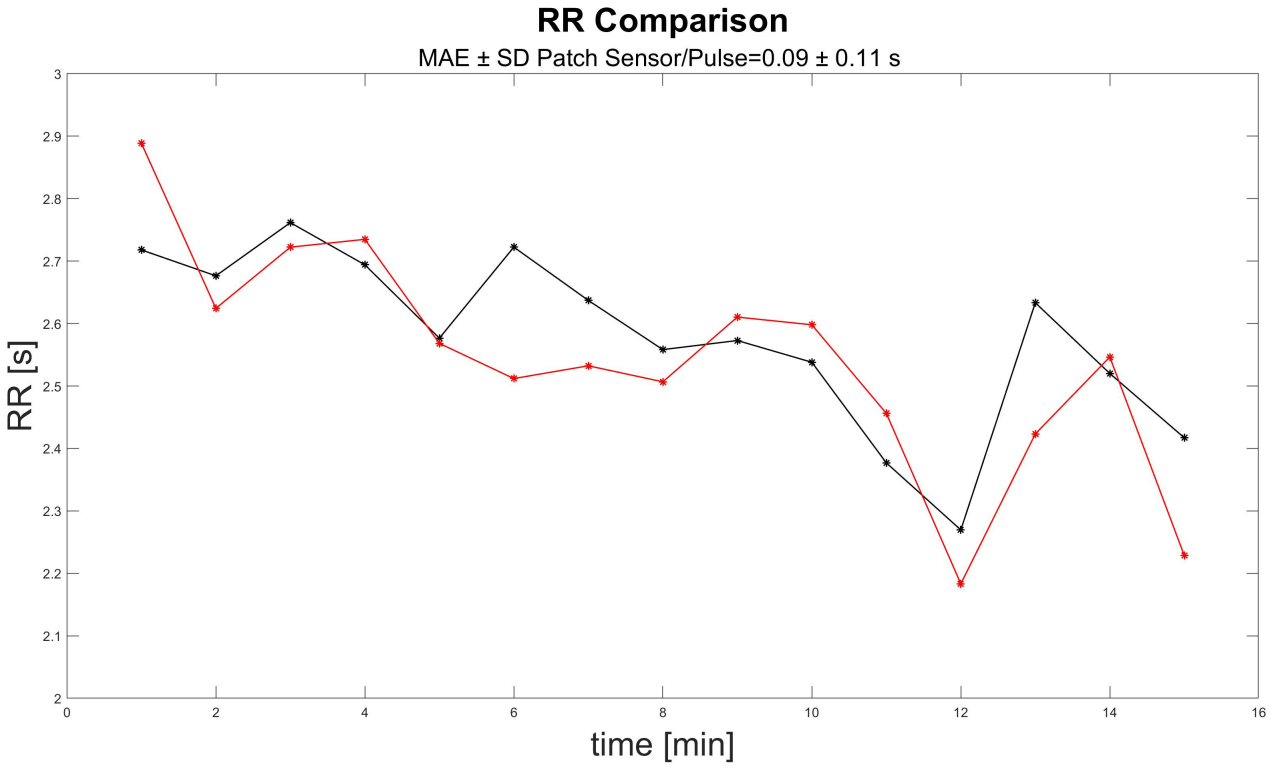

Figure 3.5: RR comparison

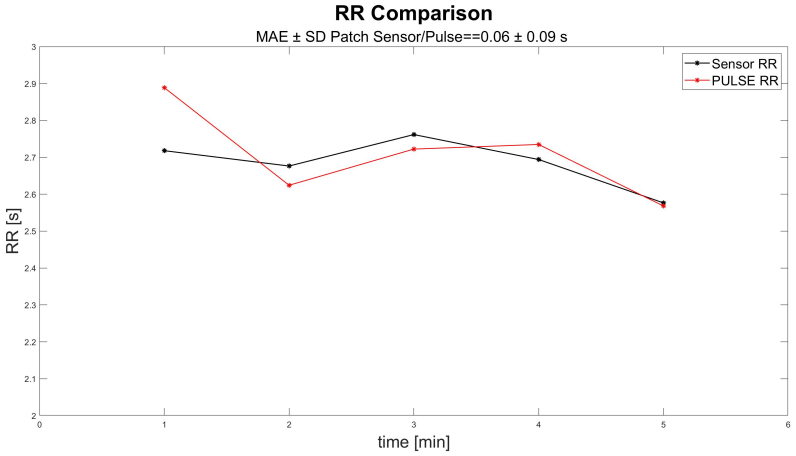

(a) *Sitting RR results comparison*

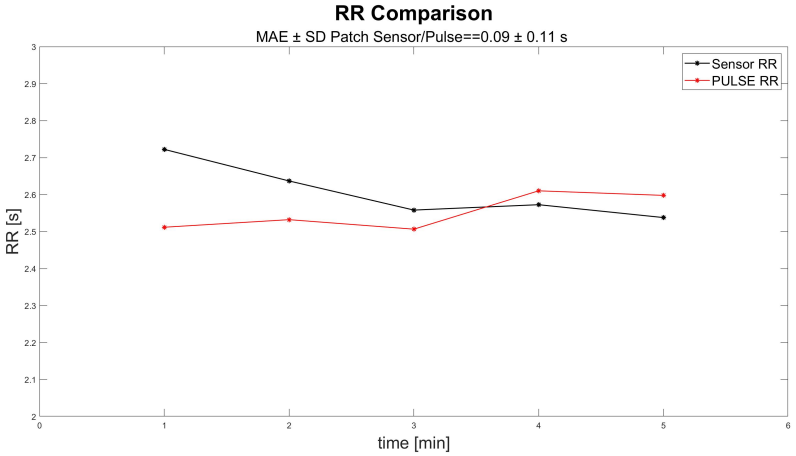

(b) *Standing RR results comparison*

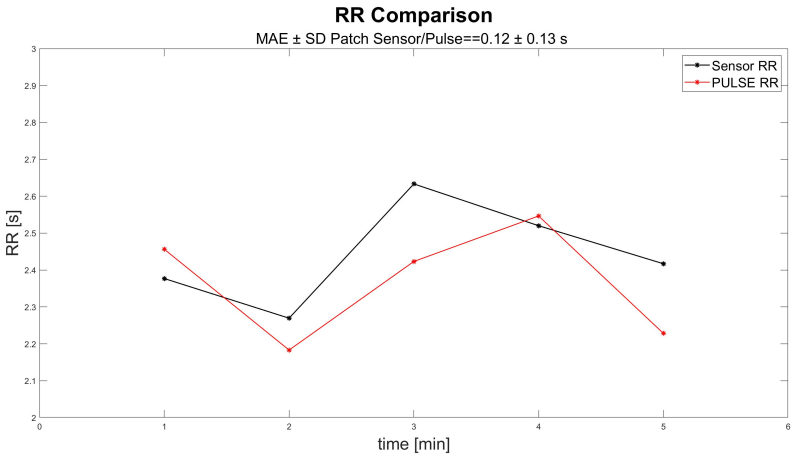

(c) *Walking RR results comparison*

Figure 3.6: Specifically comparison of RR results

3.2.3 I/E Results

The results comparison about the ratio between inhalation and exhalation (I/E) between gold standard device and patch sensor are shown below.

Trial	MAE ± SD [bpm]			
	I/E	I/E_sitting	I/E_standing	I/E_walking
1	0.05 ± 0.06	0.06 ± 0.07	0.09 ± 0.11	0.12 ± 0.13
2	0.05 ± 0.06	0.04 ± 0.05	0.08 ± 0.04	0.05 ± 0.07
3	0.13 ± 0.17	0.06 ± 0.07	0.11 ± 0.17	0.22 ± 0.25
4	0.08 ± 0.07	0.08 ± 0.12	0.05 ± 0.04	0.07 ± 0.03
5	0.07 ± 0.06	0.08 ± 0.07	0.06 ± 0.06	0.08 ± 0.06
6	0.10 ± 0.12	0.12 ± 0.14	0.06 ± 0.04	0.11 ± 0.13

Table 3.3: I/E error evaluation between patch sensor and gold standard.

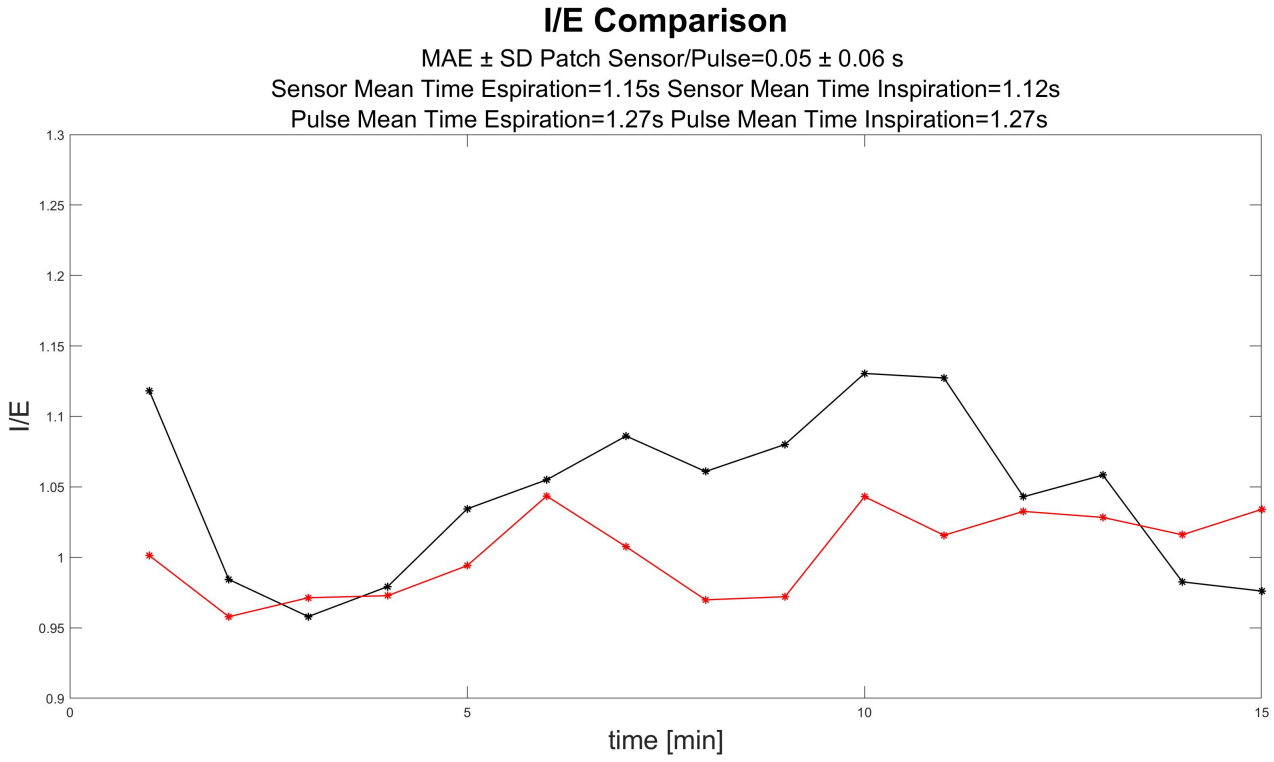

Figure 3.7: I/E comparison

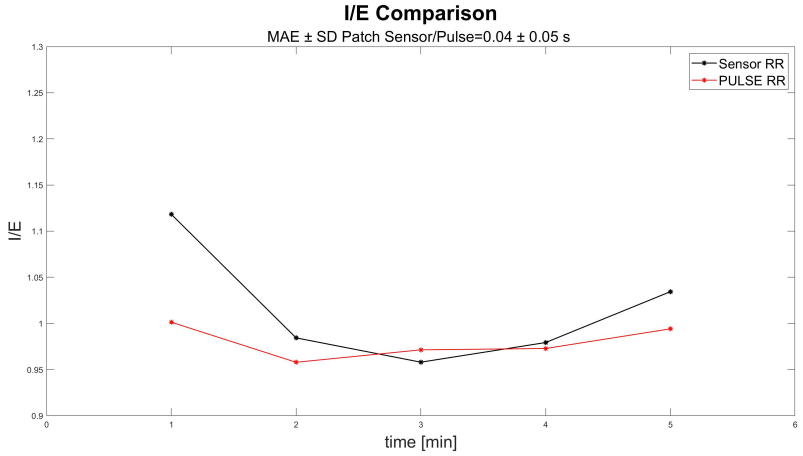

(a) *Sitting I/E results comparison*

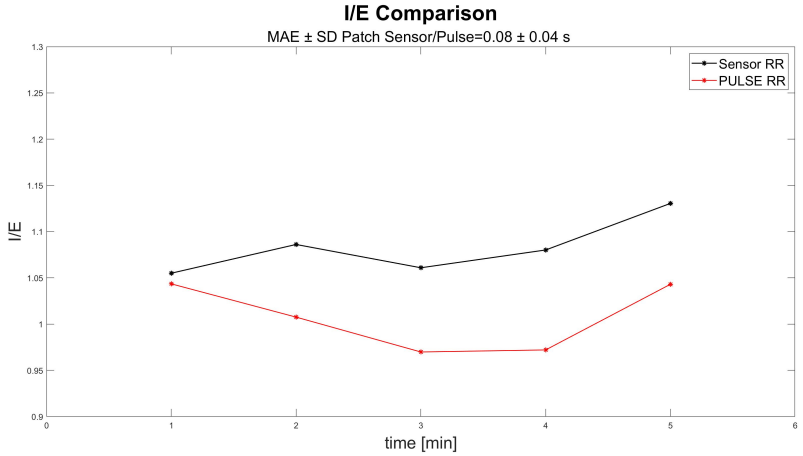

(b) *Standing I/E results comparison*

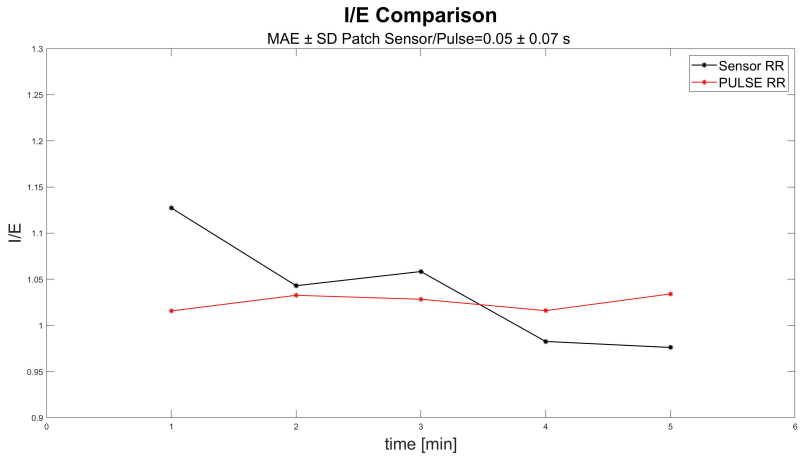

(c) *Walking I/E results comparison*

Figure 3.8: Specifically comparison of I/E results

3.2.4 Statistical Analysis

To validate the system developed, statistical analyses are performed on all complete trials according to the method followed in [41]. The BR and RR time parameters extracted by both devices are compared to investigate if there is any significant difference. Firstly, the Shapiro–Wilk test is performed on BR and RR values to investigate if they followed normal distribution. If the parameters extracted both by the Pulse and the device developed follow normal distribution (defined as $p > 0.05$ in Shapiro-Wilk test), the paired T-test is performed to investigate if there is any significant difference (defined as $p < 0.05$) between them. If normal distribution was not followed in any one group, the Wilcoxon signed-rank test (significant difference defined as $p < 0.05$) is performed as the non-parametric substitute of paired T-test.

Moreover, linear regression analysis is performed to inspect whether the correlation between the parameters extracted by using the wearable device developed and the Pulse follows a linear correlation or not. The values of one variable appear on the horizontal axis, and the values of the other variable appear on the vertical axis. The consistency is evaluated using the regression coefficient of the linear correlation R^2.

Finally, Bland-Altman plot allows to appreciate how much the system developed differs from the reference system and to verify if values estimated are in a range of confidence and, consequently, are acceptable. It is a dispersion graph used to compare two quantities of the same nature, as in this case. It does not give statistical values as solved, but by comparing the distribution of points in the plan it is possible to draw conclusions on the comparability of the two measures. The diagrams related to BR and RR are computed in Matlab and are shown in Figure 3.9(a-c).

- the difference of the two measures on the y-axis. In this case it is considered the BR and RR extracted from stretchable sensor minus the ones measured with the Pulse;
- the arithmetic mean of the two measures on the x-axis. Three horizontal lines are also plotted:
- one obtained from the average of the differences;
- two lateral lines obtained considering the average ± 1.96SD. They represent the limit of the confidence interval

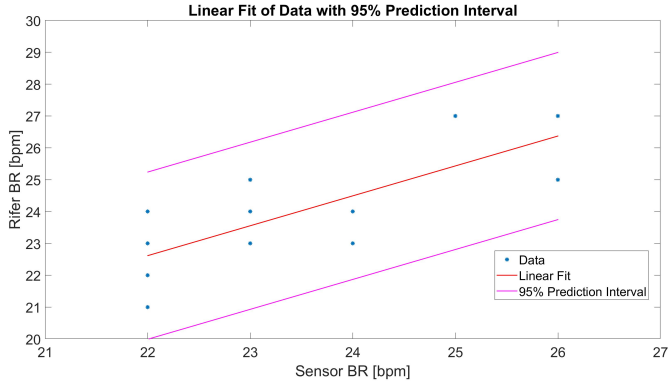

(a) *Bland Altman plot of BR results*

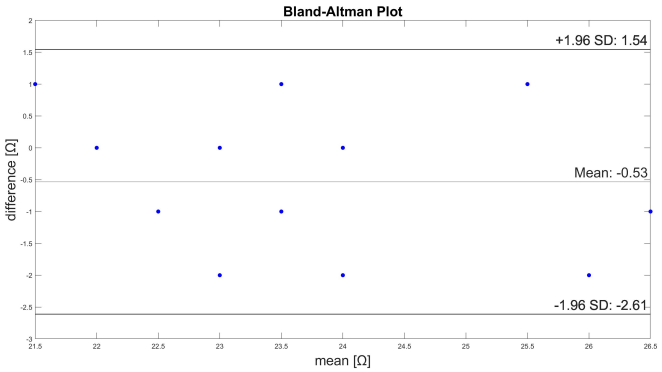

(b) *Linear Regression of BR results*

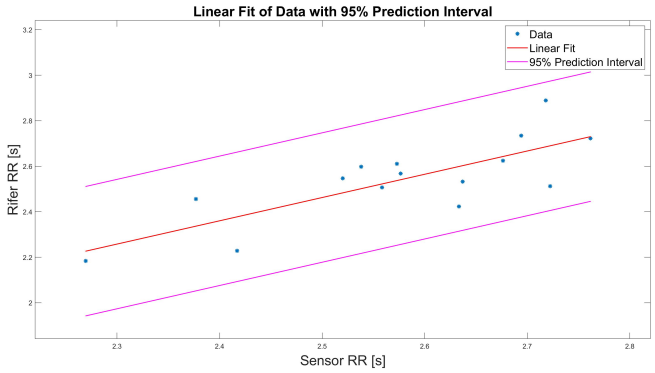

(c) *Bland Altman plot of RR results*

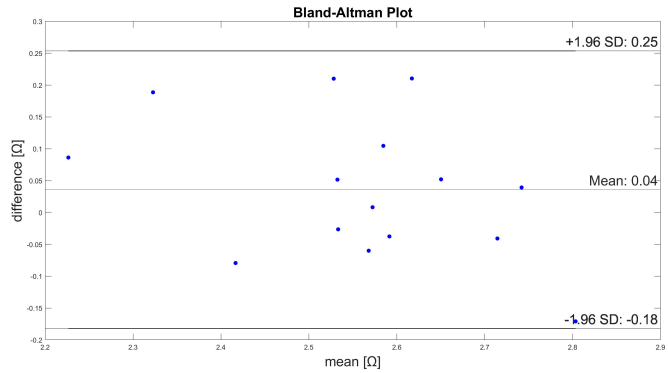

(d) *Linear Regression of BR results*

Figure 3.9: Bland Altman Plots and Linear Regression of BR and RR

3.2.5 Discussion

In this paragraph, the results of the comparison between the two devices used will be discussed.
Regarding BR, the overall error between stretchable sensor and the gold standard, defined as MAE ± SD, is 1.09 ± 1.27 [bpm]. Observing the results obtained in the different positions, the overall error measured in sitting position is 0.83 ± 0.97 [bpm]. In walking position an higher error is measured (1.15 ± 1.07 [bpm]) than standing position (1.5 ± 1.23 [bpm]). Among all the analysed trials, results obtained from the Trial 1 are representative and through them it is possible to evaluate and validate properly the accuracy of the system developed. Indeed, during the acquisition protocol, the BR value tends to increase in accordance with increasing physical activity. This is also verified by observing the decrease in the RR parameter. Its average value is lower in the walking phase than in the sitting phase. An overall error of 0.12 ± 0.14 s between the two devices is measured.
Concerning the I/E ratio, it is possible to say that this parameter remains unitary on average during the whole acquisition phase.
For all extracted parameters, a larger error was found in the walking phase.

About statistical analysis, no significance difference between the parameters extracted by the gold standard device and wearable device developed is found. In all the trials performed *pvalue* is higher than 0.05. The Wilcoxon signed-rank test is used more then paired t-test due to non-normal data distibution found thanks to the Shapiro–Wilk test.

With the Bland Altman and scatter plots can be observed the non-uniformity of the data correlations. Regarding the BR, the points on the Bland-Altman plot are scattered all over the place, it suggests that there is no consistent bias of one approach versus the other. Figure 3.9(b) shows as the device developed underestimates the BR by a value of -0,53 bpm. The calculation of 95% limits of agreement is based on the assumption that differences are normally distributed. A non-normal distribution of differences involved may not be as severe as in other statistical contexts. However, it is not required that the measures themselves follow a normal distribution [42]. A similar behaviour could be observed for RR Bland-Altman plot. In this case, however, the systematic error between the two measures is almost equal to zero.
In both diagram the points move mainly within the confidence interval and distributed symmetrically around the mean: the error distribution is not polarized.
Regarding linear regression, it is shown that all the points still move within the confidence interval. The regression coefficient R^2 evaluated is equal to 0.60 and 0.61 for BR and RR analysis respectively.

3.2.6 Critical Issues

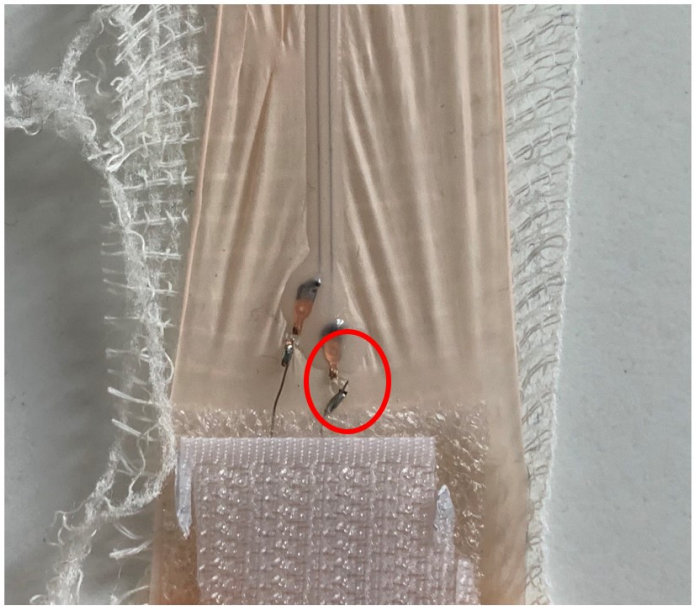

Figure 3.10: Broken contact with electrodes occurred during the breathing signal acquisition phase

During the acquisition protocol some issues have been noted.
The quality of the signal recorded by stretchable sensor is influenced by several factors. In all tested positions, due to non-adhesive sensor, the subject should maintain as straight a back position as possible. If this is not done, the sensor loses contact with the skin and the detectable impedance variations decrease. In Trial 5 it is possible that this has occurred in sitting position. Also the endurance of some patients to stay in a certain position as it caused fatigue and irritability.
Moreover, the parameters extracted from the devices are influenced by the subject's awareness of being recorded.
Finally, the copper electrodes created problems during the different acquisitions. In order to connect the sensor to the EVAL ADPD4000, these are connected with conductive wires by soldering. But, after using the sensor a few times this contact tends to break, as shown in Figure 3.10. This is probably due to the stress and the weight of the conductive wire.
To avoid this shorter and less heavy conductive wires are used.
Despite these limitations, the respiratory signals were successfully recorded in most measurements.

Chapter 4

Conclusions and future works

In recent years a strong development of telemedicine and in particular WDs has occurred. Through the use of these systems, patients can receive greater clinical support and improve their health status, communication between different users can occur even in different geographical areas, and numerous technologies can be used to provide increasingly detailed results.
Stretchable devices are the new generation of WDs. They improved the capabilities of traditional rigid electronics while maintaining epidermis-like physical properties. In this work, a wearable device to monitor respiratory rate using a stretchable sensor, developed by Uppsala University, is designed. Two evaluation boards are used to this aim. The STEVAL-STWINKT1, by STMicroelectronics, which provides timing control, data collection, and user interaction. The EVAL-ADPD4000-PPG allows measurement of changes in sensor impedance due to breathing movements through a dedicated AFE. Some hardware adjustments have been made to the latter device in order to obtain a correct exchange of information between the two evaluation boards. The polyurethane sensor used showed low hysteresis and and a linear resistance change according to the deformation.
The firmware design is developed using µVision®5 coming from Keil in C language. The STM32CubeMX software is also used to simplify programming.
The collected data are saved on sd-card and then loaded into Matlab2021a to be analyzed. Subsequently, impedance signal are filtered using a low and high pass 60 order FIR filter to mitigate the DC and the high frequency components. The delay introduced by these has been recovered. A Savitzky-Sgolay filter is also used to smooth the signal obtained.
The bioimpedance signal, collected with the Pulse sensor gold standard device, by STMicroelectronics, is processed in the same way in order to validate the sysem developed.
Respiratory parameters are extracted from both devices and the performance has been tested in different body positions, sitting, standing and walking, consecutively through 5-minute steps. They are then compared in terms of mean absolute error and standard deviation. The overall results shows an error of 1.09 $\pm$ 1.27 [bpm] in

breathing rate, 0.12 ± 0.14 s in RR time and 0.08 ± 0.09 in I/E ratio.
As [31] also demostrated, the sitting position is the one in which the best performance are obtained. Indeed, impedance variations while sitting are much more relevant than while walking.
Statistical analysis showed no significant differences in respiratory parameters extracted from the two different devices.

A new wearable device is developed using a stretchable sensor capable of monitoring breathing rate. The use of this brings with it several new features. Compared to rigid electronics, the polymer substrate tends to adapt better to skin variations. It is easy to imagine how such a sensor could be used in various healthcare environments. In addition, conductive lines formed from liquid metal can undergo large deformations. Last but not least is the lower environmental impact guaranteed by manufacturing polymer-based devices compared to classical electronics.

4.0.1 Future works

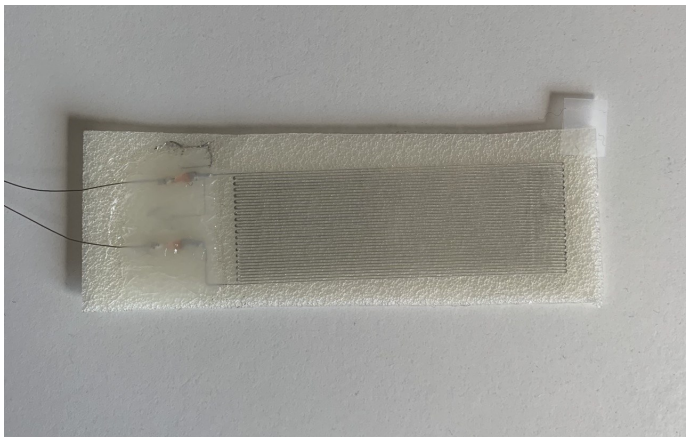

Figure 4.1: TPU stretchable sensor

Several improvements can be performed on the device developed. Some of them are listed:

- Hardware enhancements: The next step involves usingan adhesive and transparent stretchable sensor with a different pattern to improve the impedance variation. A prototype was just developed and shown in the Figure 4.1, but could not be used in this work due to several issues. In addition, the use of more stable connectors on the sensor, such as Molex connectors, instead of simple copper electrodes to facilitate the handling of the device by the user is considered.

- Firmware enhancements: configuration of other signal sensors, such as gyroscopes or accelerometers, like those on the STWIN, can improve detection of noise and motion artifacts. Furthermore, the power can be optimized;

- Software enhancements: The developed algorithm can be embedded in the microprocessor and a graphic user interface can be created for real time data visualization

Bibliography

[1] Switzerland) on Health Telematics (1997: Geneva. *A health telematics policy in support of WHO's Health-for-all strategy for global health development : report of the WHO Group Consultation on Health Telematics, 11-16 December, Geneva, 1997*. 1998.

[2] Seewon Ryu. "Telemedicine: Opportunities and Developments in Member States: Report on the Second Global Survey on eHealth 2009 (Global Observatory for eHealth Series, Volume 2)". In: *Healthc. Inform. Res.* 18.2 (2012), p. 153. ISSN: 2093-3681. DOI: 10.4258/hir.2012.18.2.153.

[3] Mohammad S. Jalali, Adam Landman, and William J. Gordon. "Telemedicine, privacy, and information security in the age of COVID-19". In: *J. Am. Med. Informatics Assoc.* 28.3 (2021), pp. 671–672. ISSN: 1527974X. DOI: 10.1093/jamia/ocaa310.

[4] Aleksandr Ometov et al. "A Survey on Wearable Technology: History, State-of-the-Art and Current Challenges". In: *Comput. Networks* 193.March (2021), p. 108074. ISSN: 13891286. DOI: 10.1016/j.comnet.2021.108074. URL: https://doi.org/10.1016/j.comnet.2021.108074.

[5] Andrea Aliverti. "Wearable technology: Role in respiratory health and disease". In: *Breathe* 13.2 (2017), e27–e36. ISSN: 20734735. DOI: 10.1183/20734735.008417.

[6] Ashraf Darwish and Aboul Ella Hassanien. "Wearable and implantable wireless sensor network solutions for healthcare monitoring." eng. In: *Sensors (Basel).* 11.6 (2011), pp. 5561–5595. ISSN: 1424-8220 (Electronic). DOI: 10.3390/s110605561.

[7] Yuhao Liu, Matt Pharr, and Giovanni Antonio Salvatore. "Lab-on-Skin: A Review of Flexible and Stretchable Electronics for Wearable Health Monitoring". In: (2017), pp. 9614–9635. DOI: 10.1021/acsnano.7b04898.

[8] J Serup, G Jemec, and G Grove. "Handbook of non-invasive methods and the skin, second edition". In: 2006.

[9] Yan Wang et al. "Standing Enokitake-like Nanowire Films for Highly Stretchable Elastronics". In: *ACS Nano* (2018), pp. 14–16. ISSN: 1936086X. DOI: 10.1021/acsnano.8b05019.

[10] Xuelin Wang et al. "Conformable liquid metal printed epidermal electronics for smart physiological monitoring and simulation treatment". In: *J. Micromechanics Microengineering* 28.3 (Feb. 2018), p. 34003. DOI: 10.1088/1361-6439/aaa80f. URL: https://doi.org/10.1088/1361-6439/aaa80f.

[11] Thao Nguyen and Michelle Khine. "Advances in Materials for Soft Stretchable Conductors and Their Behavior under Mechanical Deformation". In: *Polymers (Basel).* 12.7 (2020). ISSN: 2073-4360. DOI: 10.3390/polym12071454. URL: https://www.mdpi.com/2073-4360/12/7/1454.

[12] S. Kokare et al. "A comparative life cycle assessment of stretchable and rigid electronics: a case study of cardiac monitoring devices". In: *Int. J. Environ. Sci. Technol.* 0123456789 (2021). ISSN: 1735-1472. DOI: 10.1007/s13762-021-03388-x. URL: https://doi.org/10.1007/s13762-021-03388-x.

[13] Wikipedia contributors. *Respiratory system — {Wikipedia}{,} The Free Encyclopedia*. 2021. URL: https://en.wikipedia.org/w/index.php?title=Respiratory%7B%5C_%7Dsystem%7B%5C&%7Doldid=1019269334.

[14] J.E. Hall. A.C Guyton. "Fisiologia Medica". In: *Edises* (2007).

[15] Shelley Cazares et al. *Significance of Rib Fractures Potentially Caused by Blunt-Impact Non-Lethal Weapons*. 2017. DOI: 10.13140/RG.2.2.21169.02401.

[16] J Wanger et al. "Standardisation of the measurement of lung volumes". In: *Eur. Respir. J.* 26.3 (2005), pp. 511–522. ISSN: 0903-1936. DOI: 10.1183/09031936.05.00035005. URL: https://erj.ersjournals.com/content/26/3/511.

[17] Aleksei E. Zhdanov and Leonid G. Dorosinsky. "Modeling of estimated respiratory waveform". In: *WSEAS Trans. Environ. Dev.* 14.January 2018 (2018), pp. 383–391. ISSN: 22243496.

[18] Susannah Fleming et al. "Normal ranges of heart rate and respiratory rate in children from birth to 18 years of age: a systematic review of observational studies." eng. In: *Lancet (London, England)* 377.9770 (Mar. 2011), pp. 1011–1018. ISSN: 1474-547X (Electronic). DOI: 10.1016/S0140-6736(10)62226-X.

[19] Alejandro Rodríguez-Molinero et al. *Normal respiratory rate and peripheral blood oxygen saturation in the elderly population.* eng. Dec. 2013. DOI: 10.1111/jgs.12580.

[20] Erik Vanegas and Raul Igual. "Sensing Systems for Respiration Monitoring : A Technical Systematic Review". In: (2020).

[21] Andrea Aliverti. "Wearable technology: Role in respiratory health and disease". In: *Breathe* 13.2 (2017), e27–e36. ISSN: 20734735. DOI: 10.1183/20734735.008417.

[22] *breathing-problems @ www.webmd.com*. URL: https://www.webmd.com/lung/breathing-problems.

[23] Irisz Delestre-Levai, Virpi Sidoroff, and Richard Iles. "An Introduction to the Non-invasive Noncontact Assessment of Respiratory Function". In: *Respir. Ther.* 7 (2012), pp. 42–44.

[24] Ala'Aldeen Al-Halhouli et al. "Clinical evaluation of respiratory rate measurements on copd (Male) patients using wearable inkjet-printed sensor". In: *Sensors (Switzerland)* 21.2 (2021), pp. 1–19. ISSN: 14248220. DOI: 10.3390/s21020468.

[25] Malcolm Elliott and Alysia Coventry. "Critical care: the eight vital signs of patient monitoring". In: *Br. J. Nurs.* 21.10 (2012), pp. 621–625. DOI: 10.12968/bjon.2012.21.10.621. URL: https://doi.org/10.12968/bjon.2012.21.10.621.

[26] Xiao-Fei Teng et al. "Wearable medical systems for p-Health." eng. In: *IEEE Rev. Biomed. Eng.* 1 (2008), pp. 62–74. ISSN: 1941-1189 (Electronic). DOI: 10.1109/RBME.2008.2008248.

[27] Duarte Dias and João Paulo Silva Cunha. "Wearable Health Devices-Vital Sign Monitoring, Systems and Technologies." eng. In: *Sensors (Basel).* 18.8 (July 2018). ISSN: 1424-8220 (Electronic). DOI: 10.3390/s18082414.

[28] F Q Al-Khalidi et al. "Respiration rate monitoring methods: a review." eng. In: *Pediatr. Pulmonol.* 46.6 (June 2011), pp. 523–529. ISSN: 1099-0496 (Electronic). DOI: 10.1002/ppul.21416.

[29] Jumana Abu-Khalaf et al. "Experimental Characterization of Inkjet-Printed Stretchable Circuits for Wearable Sensor Applications." eng. In: *Sensors (Basel).* 18.10 (Oct. 2018). ISSN: 1424-8220 (Electronic). DOI: 10.3390/s18103476.

[30] Wearable Respiratory, Rate Sensor, and Printing Technology. "Fabrication and Evaluation of a Novel Non-Invasive Stretchable and Wearable Respiratory Rate Sensor Based on Silver Nanoparticles Using Inkjet". In: ().

[31] Ala Al-halhouli et al. "applied sciences Clinical Evaluation of Stretchable and Wearable Inkjet-Printed Strain Gauge Sensor for Respiratory Rate Monitoring at Di ff erent Body Postures". In: ().

[32] Ala'Aldeen Al-Halhouli et al. "Clinical evaluation of respiratory rate measurements on copd (Male) patients using wearable inkjet-printed sensor". In: *Sensors (Switzerland)* 21.2 (2021), pp. 1–19. ISSN: 14248220. DOI: 10.3390/s21020468.

[33] Michael Chu et al. "Respiration rate and volume measurements using wearable strain sensors". In: m.September 2018 (2019), pp. 1–9. DOI: 10.1038/s41746-019-0083-3.

[34] Christian Peter Subbe and Sean Kinsella. “Continuous Monitoring of Respiratory Rate in Emergency Admissions : Evaluation of the RespiraSense ™ Sensor in Acute Care Compared to the Industry Standard and Gold Standard”. In: (2018). DOI: 10.3390/s18082700.

[35] Sensortile Wireless and Industrial Node. “User manual How to use the STEVAL-STWINKT1 SensorTile Wireless Industrial Node for condition monitoring and predictive maintenance applications”. In: September (2020).

[36] Jan-hein Broeders, Healthcare Business, and Development Manager. “Wearable Market Welcomes Biomedical”. In: (), pp. 1–4.

[37] Hz Odr. “Multimodal Sensor Front End”. In: (2020).

[38] The Ld. “Ld39015 150”. In: July (2015), pp. 1–15.

[39] Wearable End Users. “A Novel Textile Stitch-Based Strain Sensor for Wearable End Users”. In: (2019).

[40] Body Gateway Electronic. “Body Gateway Electronic patch”. In: (), pp. 1–13.

[41] Al Halhouli et al. “Clinical evaluation of stretchable and wearable inkjet - printed strain gauge sensor for respiratory rate monitoring at different measurements locations”. In: *J. Clin. Monit. Comput.* (2020). ISSN: 1573-2614. DOI: 10.1007/s10877-020-00481-3. URL: https://doi.org/10.1007/s10877-020-00481-3.

[42] J M Bland and D G Altman. “Measuring agreement in method comparison studies.” eng. In: *Stat. Methods Med. Res.* 8.2 (June 1999), pp. 135–160. ISSN: 0962-2802 (Print). DOI: 10.1177/096228029900800204.